9TH CONGRESS & EXHIBITION, Asian Mining. February 15-18, 2022. Kolkata, India

TUNNELS, CAVERNS AND SLOPES IN DISCONTINUA – A CRITICAL ASSESSMENT OF CONTINUUM ANALYSES, GSI, HOEK-BROWN AND MOHR-COULOMB, WITH FOCUS ON DISCONTINUUM ANALYSES AND GEOLOGY

Nick Barton, NB&A, Oslo, Norway (www.nickbarton.com)

Abstract

Rock masses are by definition assemblies of rock blocks separated by joint sets and less frequent faults. Over the years quite accurate methods have been developed for numerical modelling of these assemblies, both in 2D (UDEC-MC, UDEC-BB) and in 3D (3DEC-MC). We have used them for studying how tunnels, caverns and slopes perform when excavated in these challenging media. Empirical characterization methods have also been developed which can assist in such activities as tunnel and cavern support, and stope dimensioning. These can complement the numerical modelling. Clearly, open pit slopes in jointed rock are not the same as model slopes in unjointed model materials. We are readily able to observe the differences between real failures and modelled failures. Two key problems seem to be the over-simplicity of GSI and the black-box complexity of Hoek-Brown et al equations. Related codes using M-C parameters derived from H-B seem also to be affected. A return to joint and rock mass characterization for discontinuum models is needed if we are to return closer to reality. We made good progress in rock engineering many decades ago, until too many chose GSI and H-B, the easy way to lose sight of real behaviour since no 'geology'.

Introduction

In this lecture the author will be showing studies with UDEC, 3DEC, FLAC and FLAC3D, in illustrating both discontinuum and continuum analyses for tunnels, caverns and open-pit slopes. The use of the first four parameters of Q for assisting in stope dimensioning will also be briefly addressed – and just two for overbreak.

Having been around for a long time, also as a student colleague of Cundall before he developed his remarkable computer codes, it perhaps is permitted to illustrate briefly what we could achieve with physical models of fractured media *before Cundall's codes became available,* both from thesis times in 1971 and from just prior to Cundall's UDEC release (Barton, 1971, Barton and Hansteen, 1979).

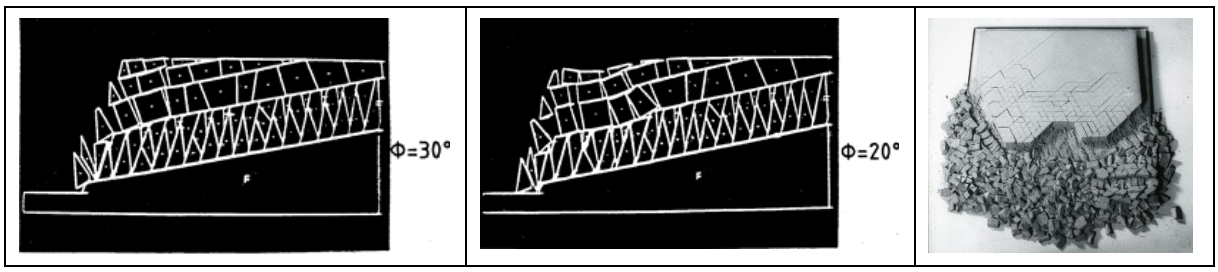

Figure 1 The contrasting flexibility of the intelligent computer code µDEC: two of four results of varying angle Φ from Cundall, Voegele and Fairhurst, 1975, and the 'fixed-fracture-sets' fractured 2D models developed some years earlier by the author in 1968. Coming just before UDEC such 2D 'slab models' with 4,000, 1,000 and 250 blocks also assisted in scale effect understanding. The smallest block sizes gave unexpected 'linear' stress-strain behaviour.

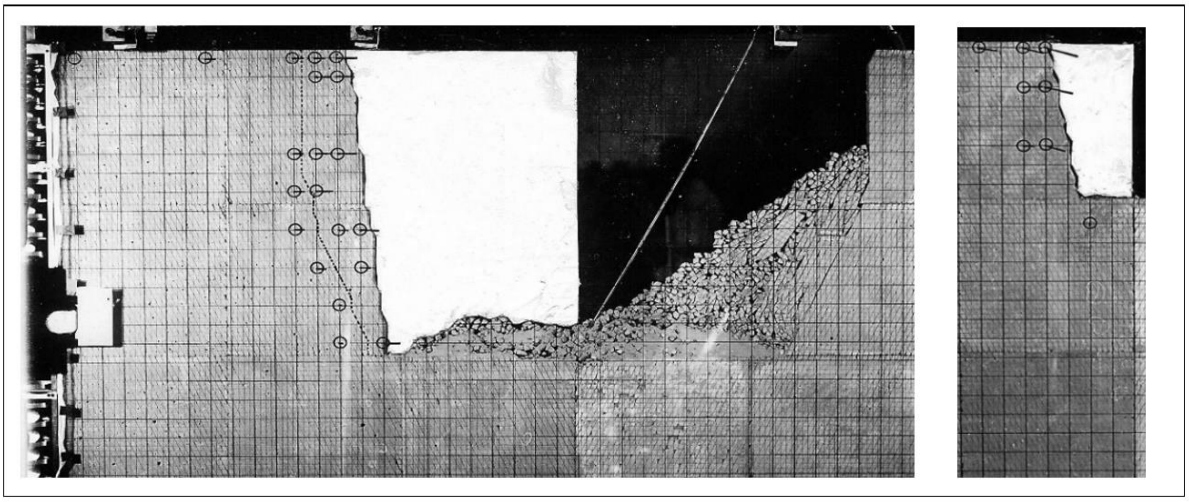

Figure 2 Physical 2D 'wall models' of fractured slopes with an initial 40,000 blocks and high or low horizontal stress applied at the boundaries prior to excavation. Deformation vectors were recorded by photogrammetric analysis. (Barton, 1971).

The 'reluctance' to reach slope failure until very steep slopes were excavated as seen in Figure 2 was due to the increment of shear strength caused by *over-closure*. This is a feature of rough joints that has implications for geothermal reservoir and CO_2 sequestration, due to the related *thermal-over-closure* component of rock joint resistance, if such are sufficiently rough: probably with JRC > 10. (Barton, 2020).

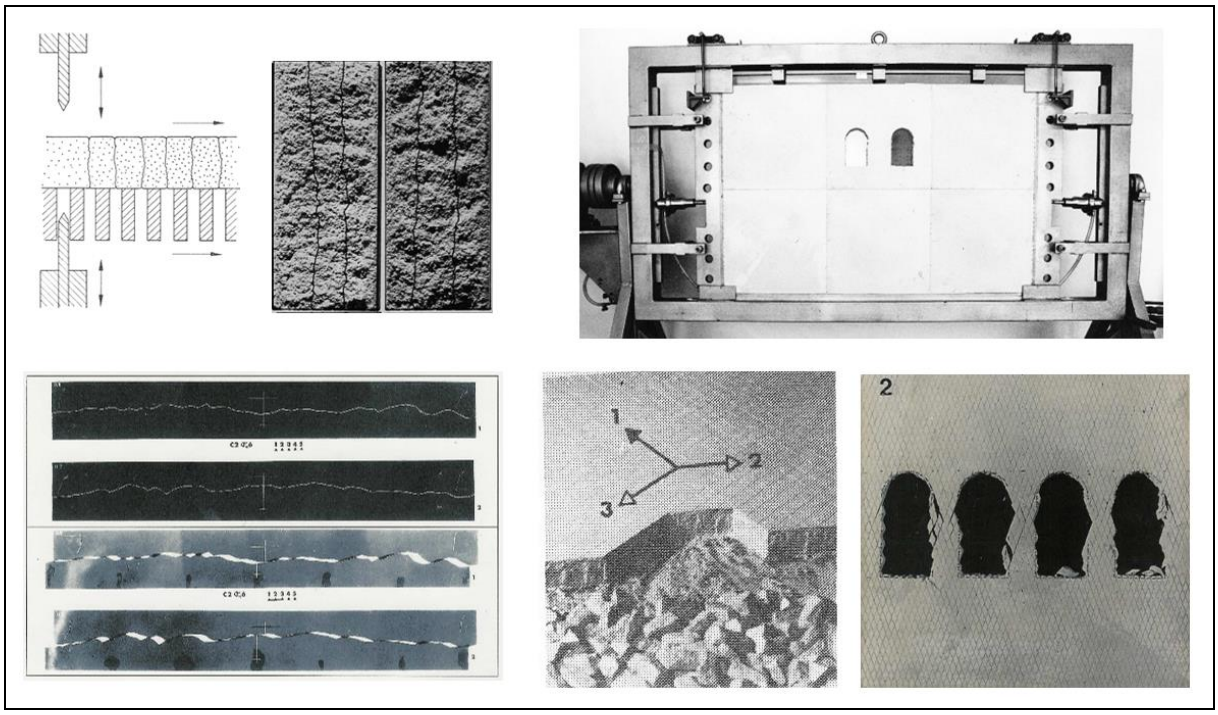

Figure 3 The principal mechanism of tension-fracture model development and their roughness are illustrated on the left. A subsequent underground simulation series by Barton and Hansteen, 1979 (my NGI colleague providing the continuum model comparisons) is shown on the right. One year after publication of these UNPP studies, UDEC became available. The writer has no regrets. It is a special feeling: 'registering' stress concentration when excavating with 'sharpened-tube-and-vacuum' methods in cavern arches and inverts.

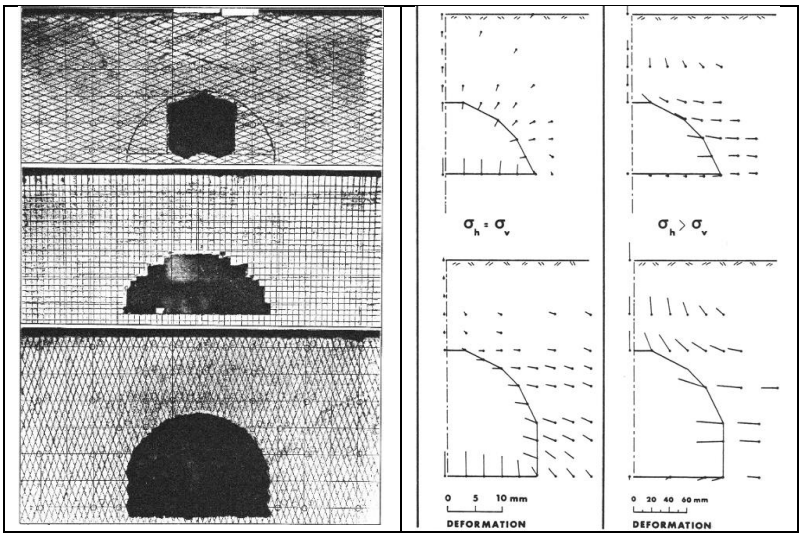

Figure 4 Cavern models were excavated in four different fracture-set formats. The 0º/90º variety (central photo) could have primary (continuous) fracturing horizontal or vertical. The secondary set (also cut with the double-bladed guillotine) has perpendicular steps where crossing set #1. The elastic continuum FEM models correspond to the models in Figure 5.

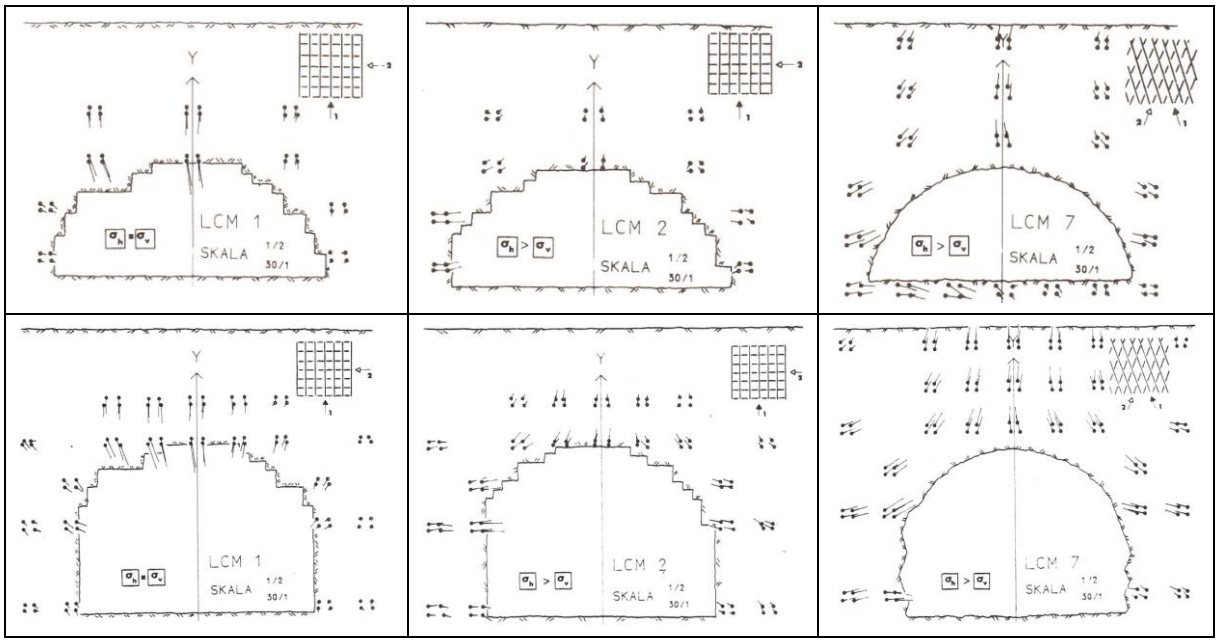

Figure 5 A selection of the cavern models which were studied in the pre-UDEC period, in order to evaluate the feasibility of underground nuclear power plant (UNPP) spans of 50m. The deformation vectors show the importance of horizontal stress and demonstrate the inadequacy of continuum modelling, even when fracture shear strengths are high, and stability is good without support being needed. Barton and Hansteen, 1979.

Some of these early pre-UDEC physical fracture models are reproduced in this lecture as they still appear not to have been repeated and represent a ‘physical reality’ even though not a ‘geological reality’. They may serve as code verification objects. In the end the early UNPP studies in Norway came to nothing, and Sweden (who had part-funded these studies through BeFo) built surface nuclear plants, while Norway continued with the most extensive underground hydroelectric developments.

Some fundamentals of joint behaviour

The physical fracture models suggested some differences to continuum modelling, with joint orientations being particularly important. In Figure 6 we can see a more fundamental feature of joint behavior. The four caverns were excavated one after the other in a high horizontal stress situation, as in four of the cases in Figure 5. Of particular note is the hysteresis or ‘deformation set’ seen in the narrow pillars. The photogrammetry-determined deformations did not reverse noticeably, when a new cavern was excavated, as would have happened in an elastic continuum model.

Figure 6 A multi-cavern experiment with ultra-narrow pillars, prior to model earthquake loading monitored with an accelerometer (a scaled 0.1 to 0.7g). Figure 3, bottom right, shows the cavern degradation during ‘the earthquake’. Note the deformation vectors in the pillars are not reversing as they would in a continuum model. In the next figure we see that three styles of joint deformation may occur with jointed rock masses and each have been recorded in in situ loading tests. They are absent from conventional continuum modelling.

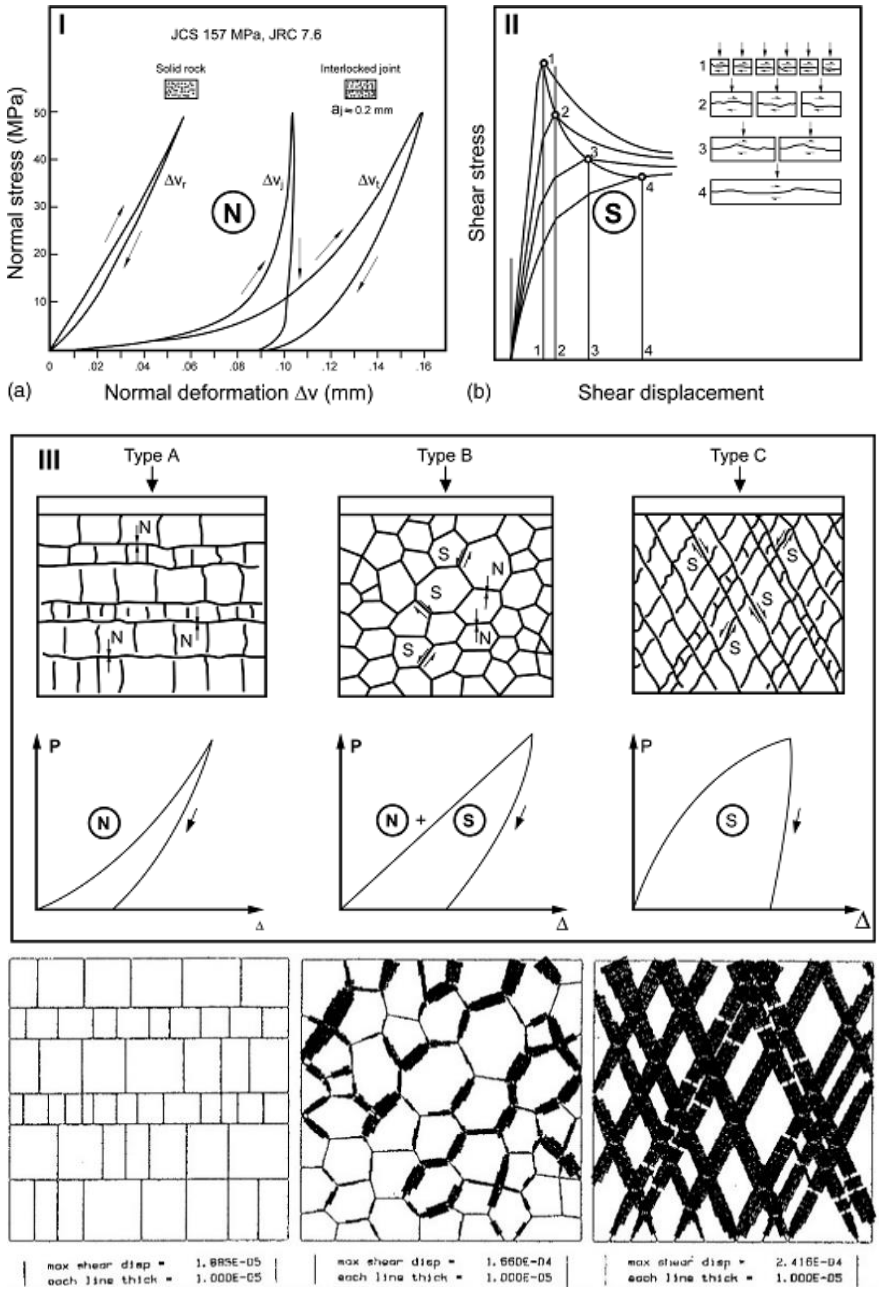

Figure 7 The N (normal) Type A concave deformation and the S (shear) Type C convex deformation, with the combined mode Type B seen in loading tests across columnar basalt. An NGI colleague from the late 1980's matched these three styles using UDEC-BB after this code became available in 1985. Note the normal stress-joint closure curves from Bandis et al. 1983 and the shear stress-displacement curves (with scale effects) from Bandis et al. 1981. The N and S and N+S loading suggestions for the three rock mass assemblies are from Barton, 1986.

To state the obvious there are no continuum model or GSI-based Hoek-Brown equations to match the essentially discontinuous behaviour shown in any of the above figures, which perhaps GSI users can be happy about, as it makes their rock engineering practice significantly easier. But was the practice of rock mechanics for rock engineering supposed to be easy? The use of GSI and continuum models has taken the realism out of the subject, which perhaps was not the original intention of Hoek and Bray and Hoek and Brown: these were classically helpful textbooks.

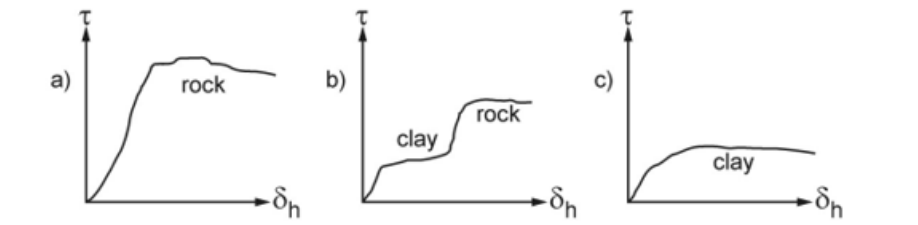

(a) Rock wall contact (thin coatings)

	Jr	Ja = 0.75	1.0	2	3	4
		$\tan^{-1}(Jr/Ja)^o$				
A. Discontinuous joints	4	79°	76°	63°	53°	45°
B. Rough, undulating	3	76°	72°	56°	45°	37°
C. Smooth, undulating	2	69°	63°	45°	34°	27°
D. Slickensided, undulating	1.5	63°	56°	37°	27°	21°
E. Rough, planar	1.5	63°	56°	37°	27°	21°
F. Smooth, planar	1.0	53°	45°	27°	18°	14°
G. Slickensided, planar	0.5	34°	27°	14°	9.5°	7.1°

(b) Rock wall contact when sheared (thin fillings)

	Jr	Ja = 4	6	8	12
		$\tan^{-1}(Jr/Ja)^o$			
A. Discontinuous joints	4	45°	34°	27°	18°
B. Rough, undulating	3	37°	27°	21°	14°
C. Smooth, undulating	2	27°	18°	14°	9.5°
D. Slickensided, undulating	1.5	21°	14°	11°	7.1°
E. Rough, planar	1.5	21°	14°	11°	7.1°
F. Smooth, planar	1.0	14°	9.5°	7.1°	4.7°
G. Slickensided, planar	0.5	7°	4.7°	3.6°	2.4°

(c) No rock wall contact when sheared (thick fillings)

	Jr	Ja = 5	6	8	12	13	16	20
		$\tan^{-1}(Jr/Ja)^o$						
Nominal roughness of discontinuity rock walls	1.0	11.3°	9.5°	7.1°	4.8°	4.4°	3.6°	2.9°

Figure 8 Variations in the shear strength of unfilled, clay-coated, and clay-filled discontinuities as illustrated here from the Q-system, cannot be included in GSI in a 'free manner' independent of joint roughness, because the use of Bieniawski's joint condition factor does not make such differentiation possible. The 'joint condition' moves in one direction, so rougher joints cannot have clay coatings or fillings. Barton, 2002.

Some illustrative examples of UDEC-BB models with geological detail

In the following rather concentrated 'gallery' of discontinuum models we will show features of potential behaviour that can hardly be matched in any way by continuum modelling. The exception – to a degree – is the redistribution of stress, from principle far-field stresses to tangential and radial stresses. The rotation of the small 'crosses' we also see clearly in continuum models, but the loading of bolts where they cross and support wedges, and the unstressed unstable wedges are not of course seen in continuum models. The discontinuum model teaches us to look out for behaviour that is absent from continuum modelling, unless we are happy perhaps with a colour-plot change. In UDEC-BB we see the distribution of joint shearing and also the stress or depth dependent physical and JRC-estimated hydraulic apertures, for H-M modelling.

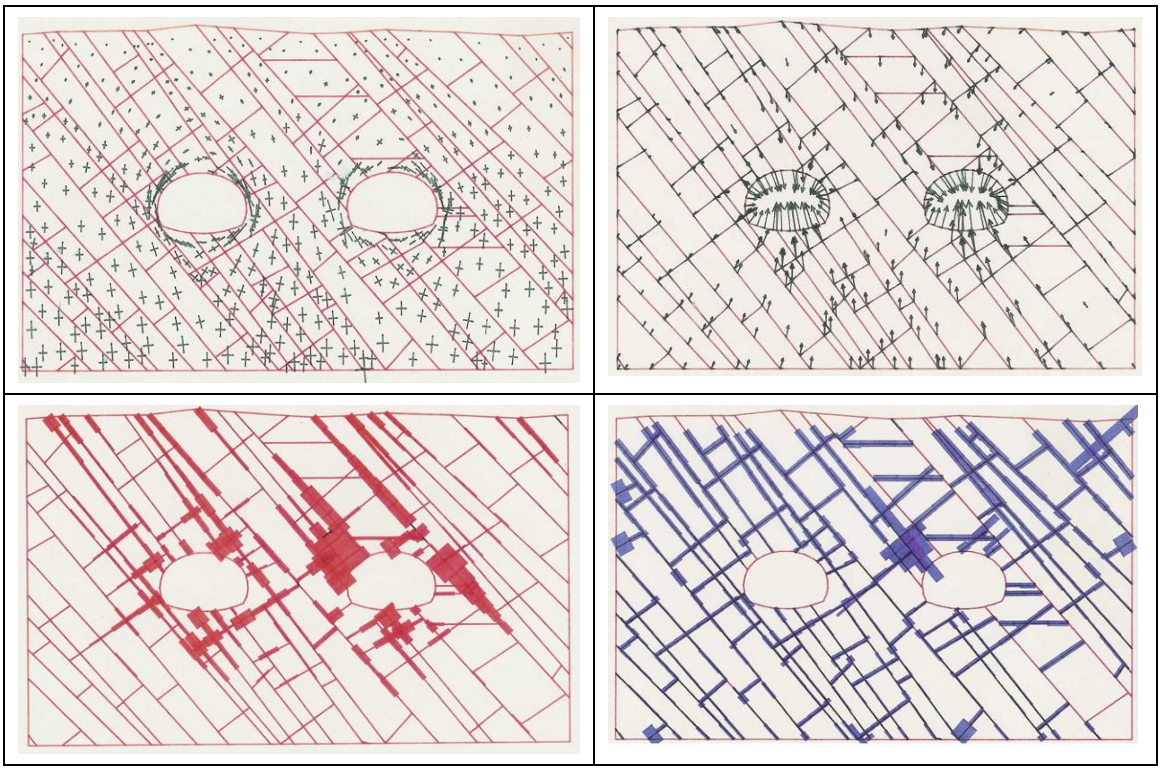

Figure 9 Early UDEC-BB models of the Fjellinjen (Oslo) tunnels by Makurat and Barton, 1988. The discontinuum details (joint shearing and joint apertures) are not in continua.

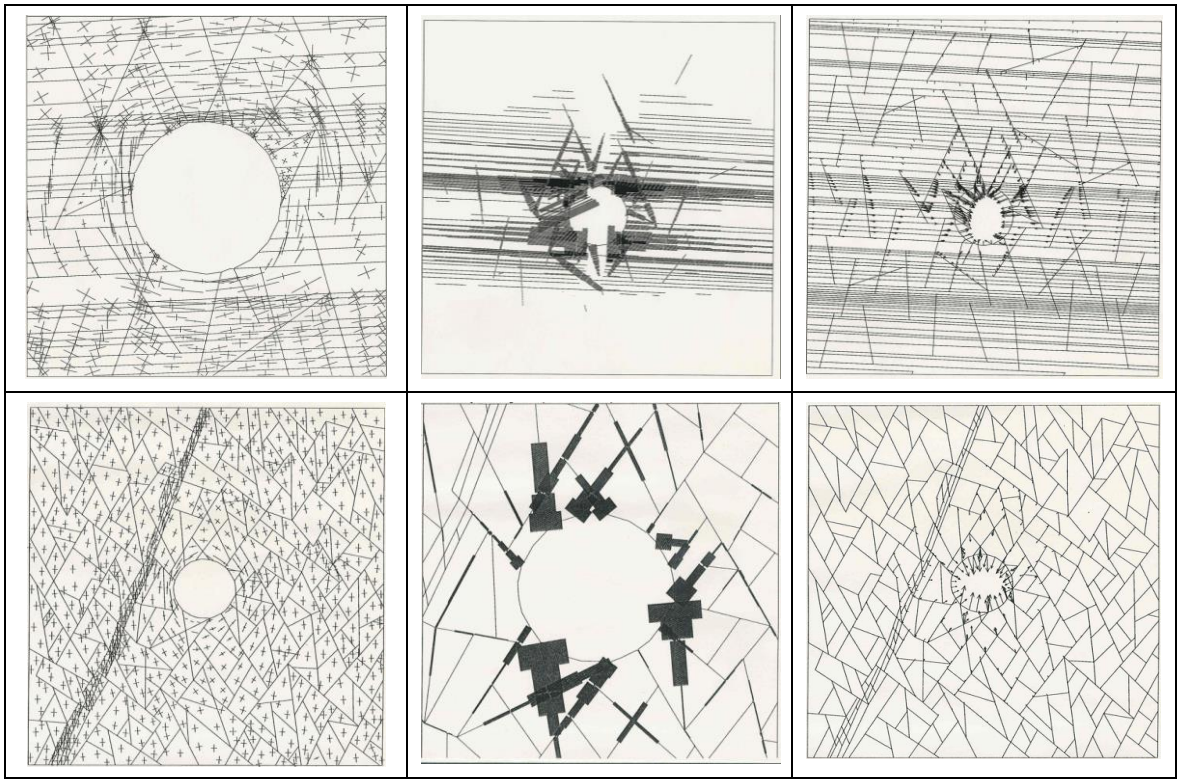

Figure 10 UDEC-BB studies of 250m deep and 700m deep TBM spiral access tunnels through the interbedded St Bees sandstones and siltstones (top) and through the Borrowdale welded tuffs-ignimbrites (bottom) at the planned Sellafield LLW/ILW nuclear waste repository, from 1992. Thanks to NGI's numerical modelling team, during our 6 years consultancy for UK Nirex, 1990-1996.

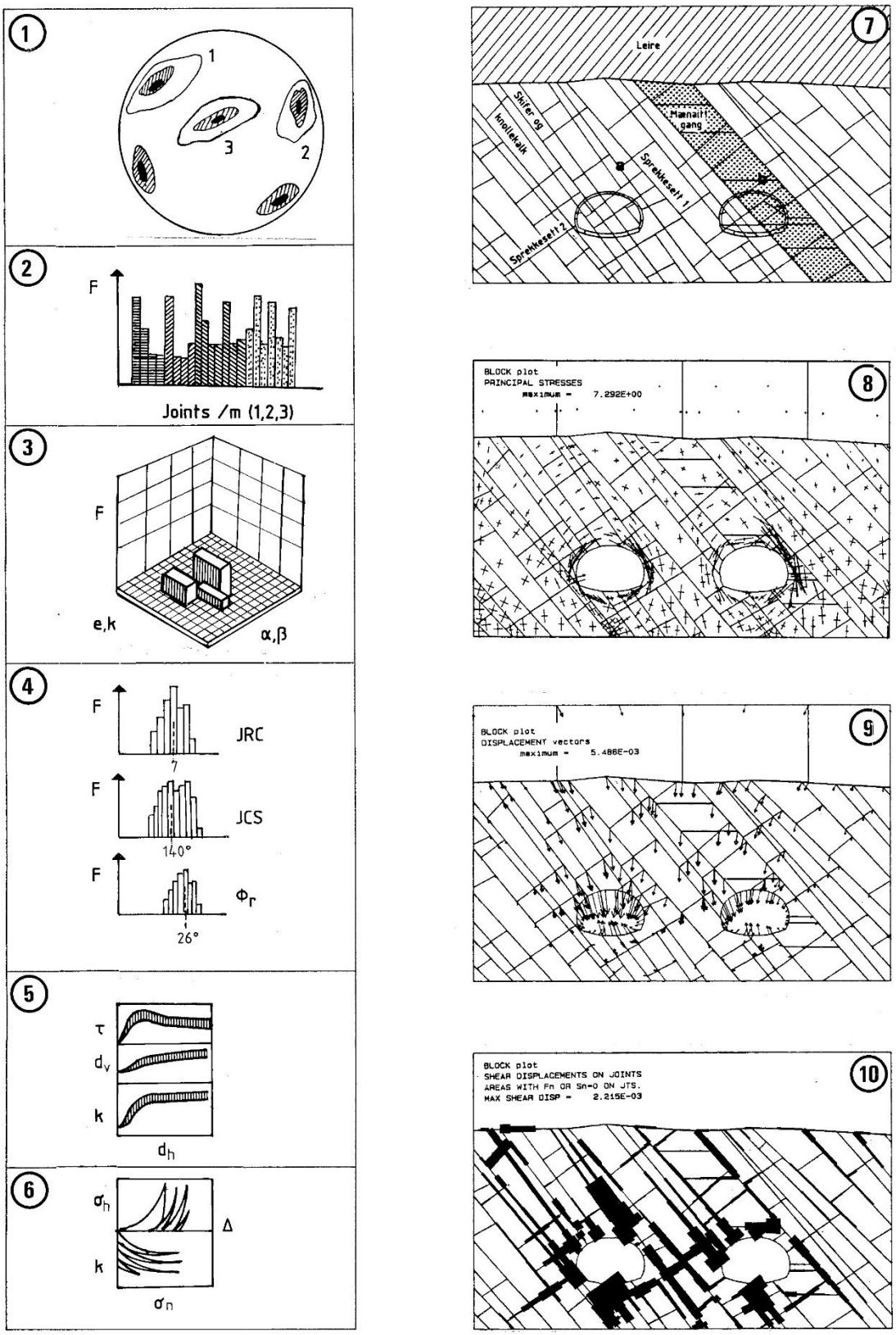

Figure 11 A glimpse of the principles of discontinuum modelling input data operations: joint orientations and frequencies, permeability and aperture estimation (but this will be estimated by UDEC-BB) and joint index test results for JRC, JCS and φ_r. Boxes 5 and 6 symbolize the shear stress-displacement-dilation-permeability and normal stress-closure operations of the Barton-Bandis model. (see Barton, Bandis, Bakhtar, 1985 and Barton, 2021 for examples).

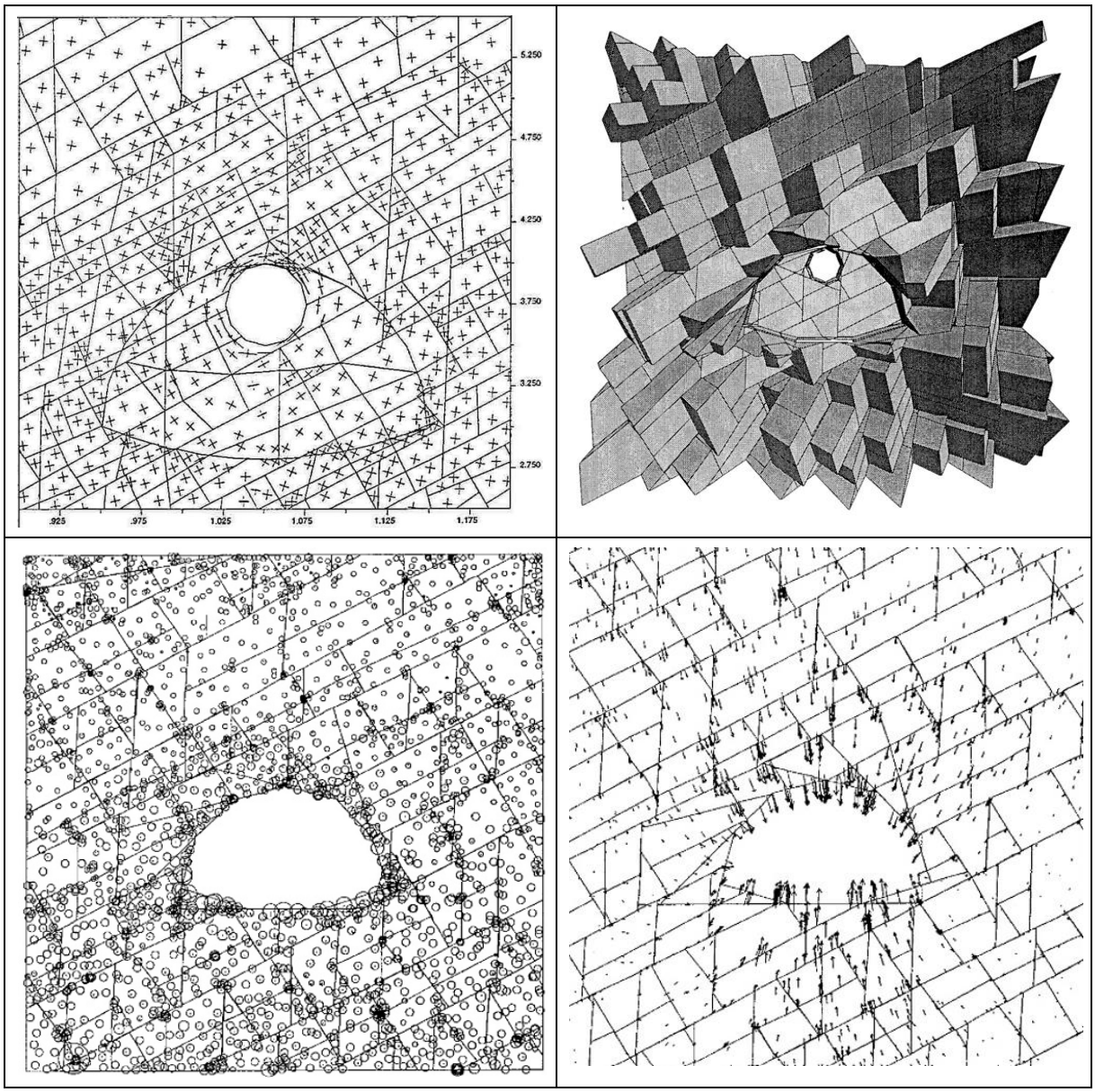

Figure 12 Top left: UDEC-BB to check TBM pilot tunnel break-out to full section. The 3DEC sections show a maximum tangential stress of 7.9 MPa and a maximum displacement of 8.0mm. This project is illustrated further in the next figure.

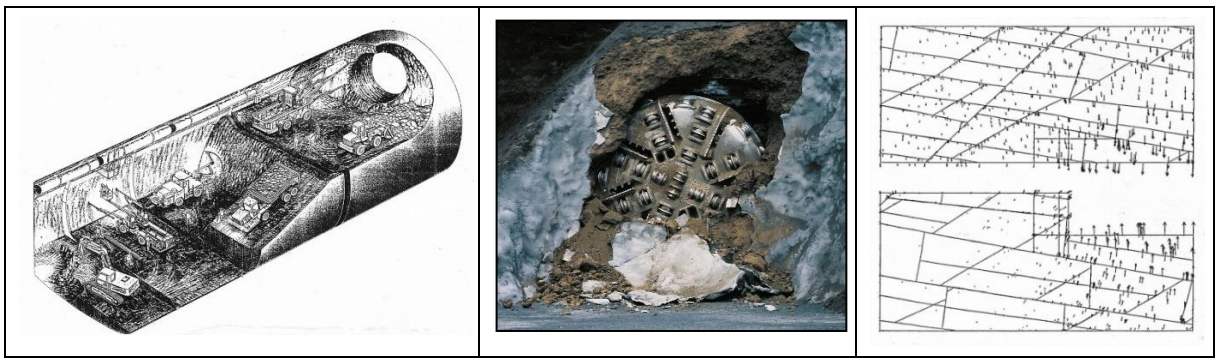

Figure 13 The unusual motorway pilot-TBM for the Tokyo-Osaka Tomei 2 Shimizu 3 motorway project. The TBM could turn so as to provide a pilot bore for the parallel tube. NGI UDEC-BB and 3DEC modellers from the late 1980's included Marte Gutierrez, for Dr J. Itoh.

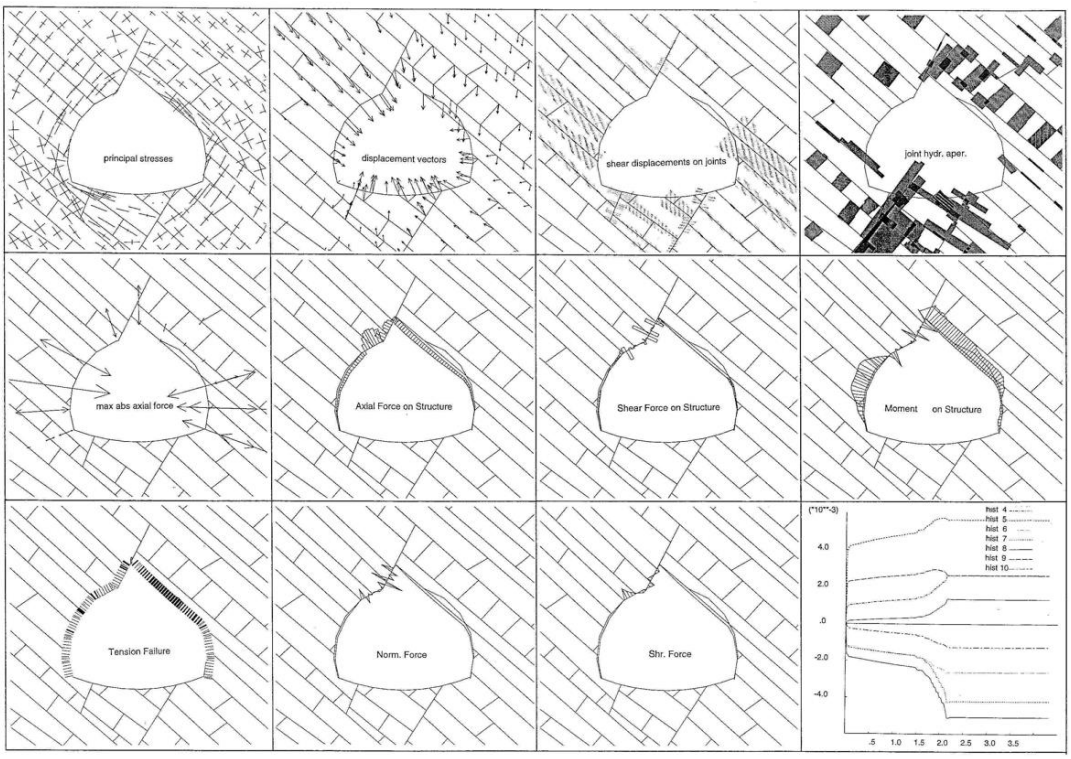

Figure 14 The discontinuum-modelling advantages of representing adversely steeply-dipping bedding. This late 1980's UDEC-BB model is from one of NGI's Japanese consulting projects that was managed by the writer. The model showed distinct signs of over-loading of the bolting. The bonding failure of the modelled S(fr) is also shown, bottom left.

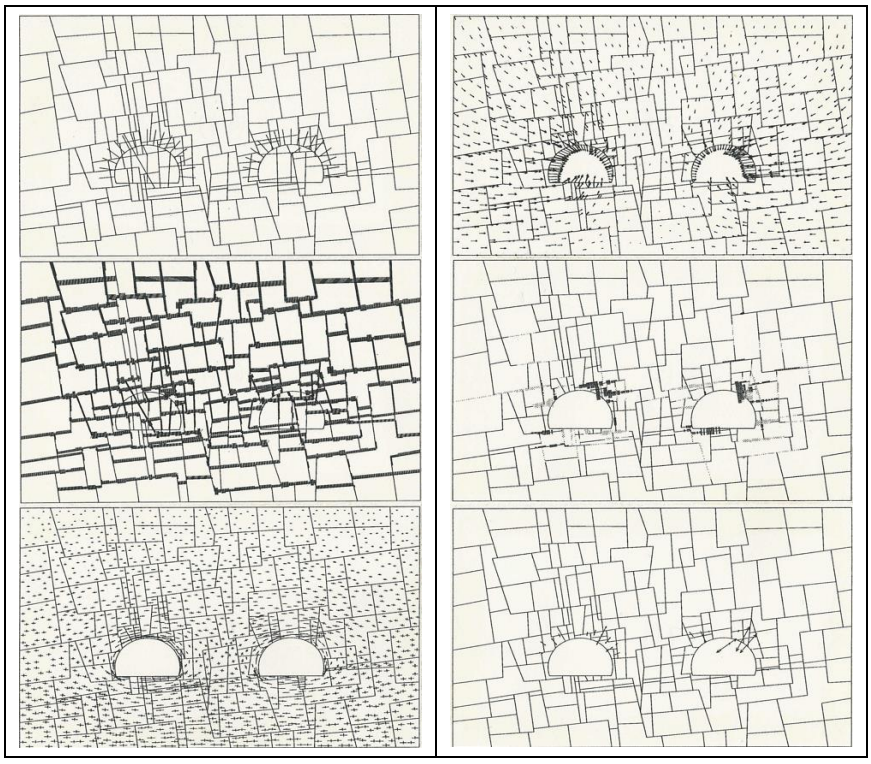

Figure 15 The twin motorway tunnels of Tsing YI between Hong Kong and the new airport. The UDEC-BB model needed joint observation and index test estimation for JRC, JCS and φ_r. Geometry, deformations, joint apertures, joint shearing, stresses and bolt loads are shown. NGI contract for the tunnel contractor, early 1990's. The writer was project manager.

A particularly important discontinuum modelling contract was the NGI design check for the designers of the 62m span Gjøvik Olympic cavern. This was done on behalf of owner Fortifikasjon, whose director Jan Rygh had drawn the ‘classic serviette sketch’ for the town’s chief planning engineer some years earlier, before the winter games were awarded to nearby Lillehammer.

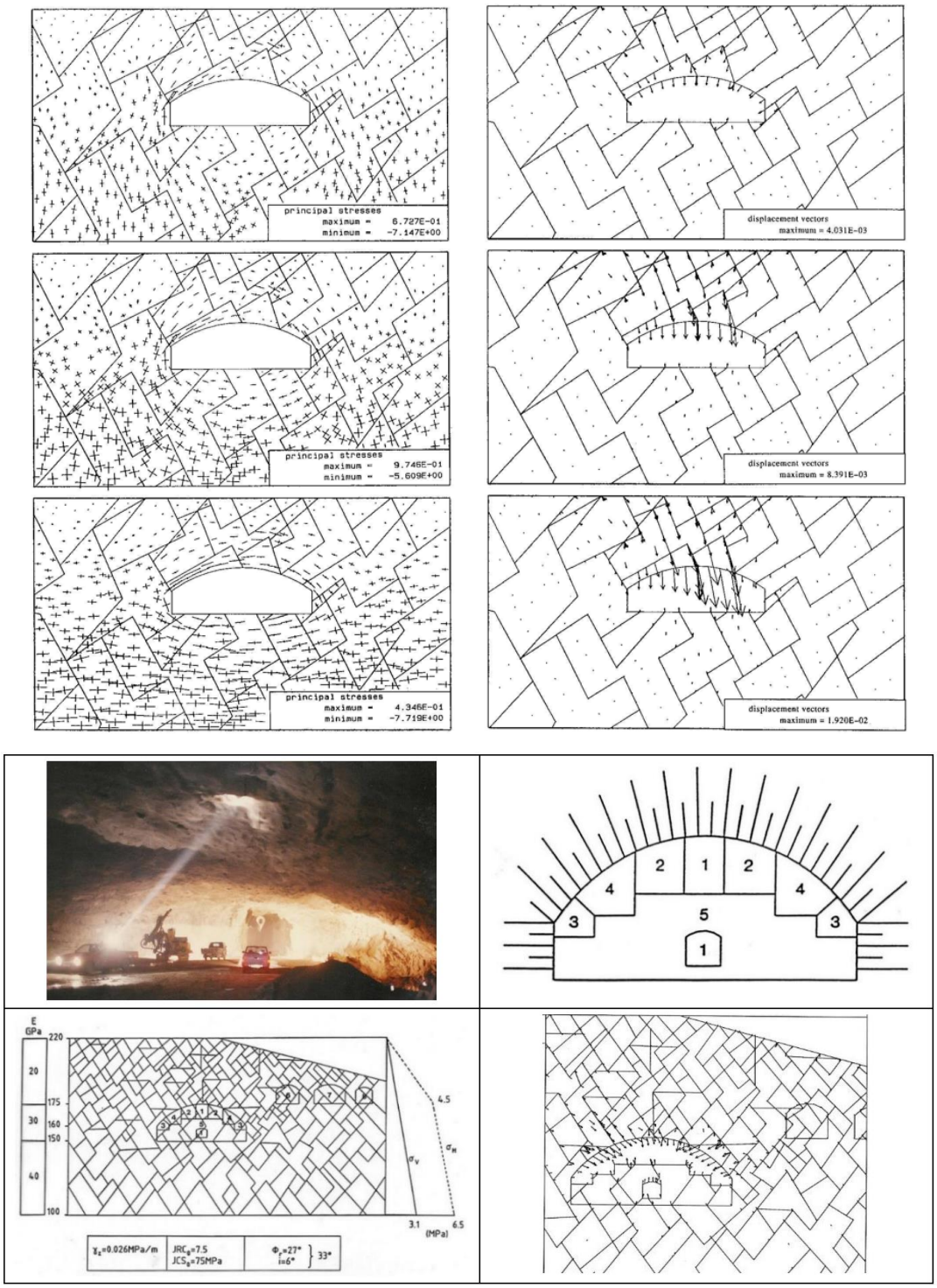

Figure 16 Sensitivity studies conducted by Tunbridge, and subsequent detailed UDEC-BB modelling by Chryssanthakis, for the 62m span Gjøvik cavern. Note multi-author NGI reference due to Q-logging, cross-hole seismic tomography and rock stress measurement. Barton, Chryssanthakis, Tunbridge, Kristiansen, Løset, Bhasin, Westerdahl, Vik, 1994.

Overbreak and tunnel and stope stability

A feature of excavation effects in rock masses that particularly marks the stark difference between continuum and discontinuum modelling is *overbreak*. In Barton, 2007 it was suggested that this could be quantified by the Q-parameters ratio Jn/Jr. Figure 17 (top photos and roughness sketches) shows how this works. The red-coloured ratios show Jn/Jr < 6, while the blue-coloured ratios show Jn/Jr ≥ 6 which is the suggested criterion. Q-parameter statistics at the LKAB mine (coloured sketches) explain the overbreak. Elevated values of Ja (clay coatings) add to the problem.

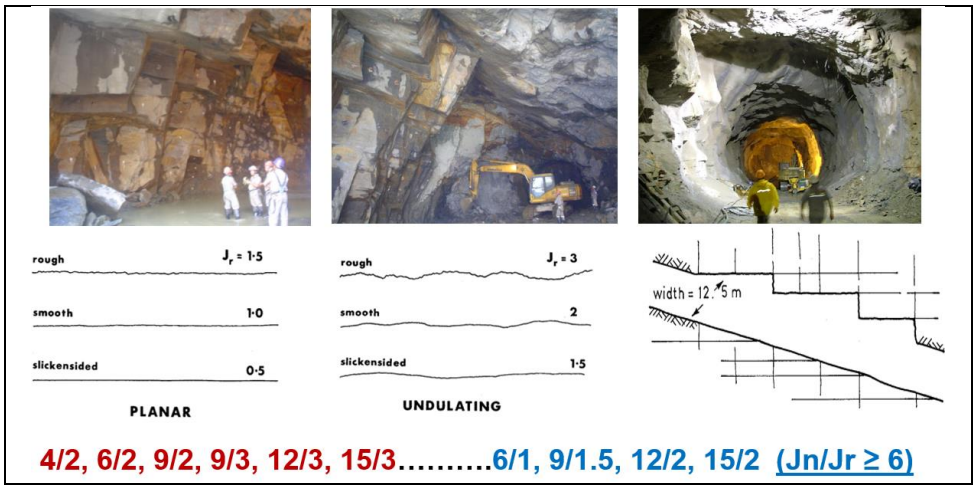

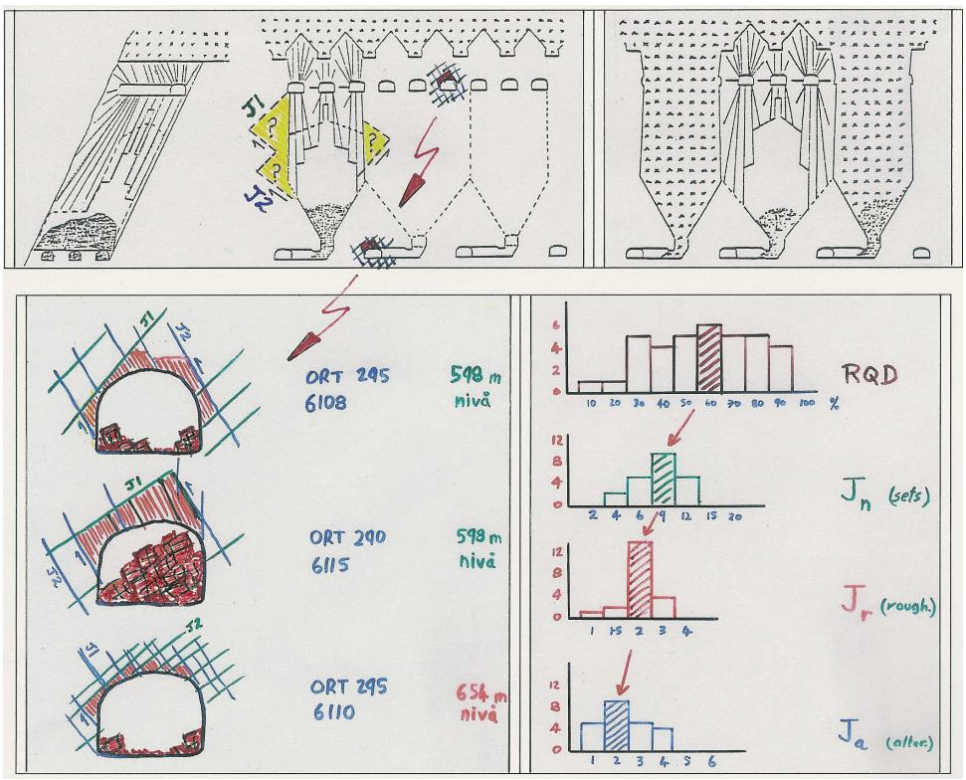

Figure 17 Top: the Q-parameter ratio Jn/Jr ≥ 6 suggests almost unavoidable overbreak if there are sufficient degrees of freedom for block fall-out (higher Jn) and if joint roughness is low enough (low Jr). Bottom: observations performed by the writer in 1988 in LKAB's Oscar long-hole drilling stope-development project in Kiruna in northern Sweden. Explanations for the excessive overbreak were sought. This was the first time that Q-parameter histograms were used by the writer, and soon this became a systematic way of logging Q.

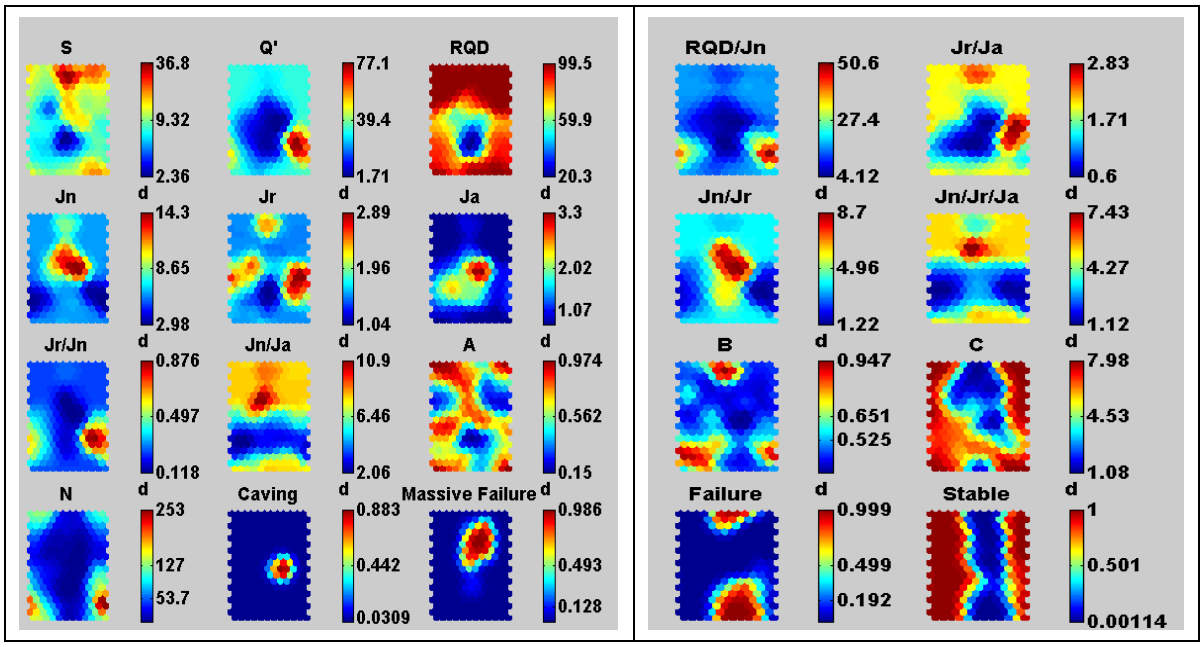

Figure 18 This 'graphical matrix' scheme developed by Dr Fraser of CSIRO, was shown to the writer during a two-days rock engineering course in Melbourne in 2005. The subject matter is stoping, and stable, caving, failure and massive failure are the operative terms. The relative influence of various separate and combined Q-parameters are taken from the Potvin scheme of utilizing Q' = RQD/Jn x Jr/Ja in mine-stope dimensioning. Next figure shows ABC:

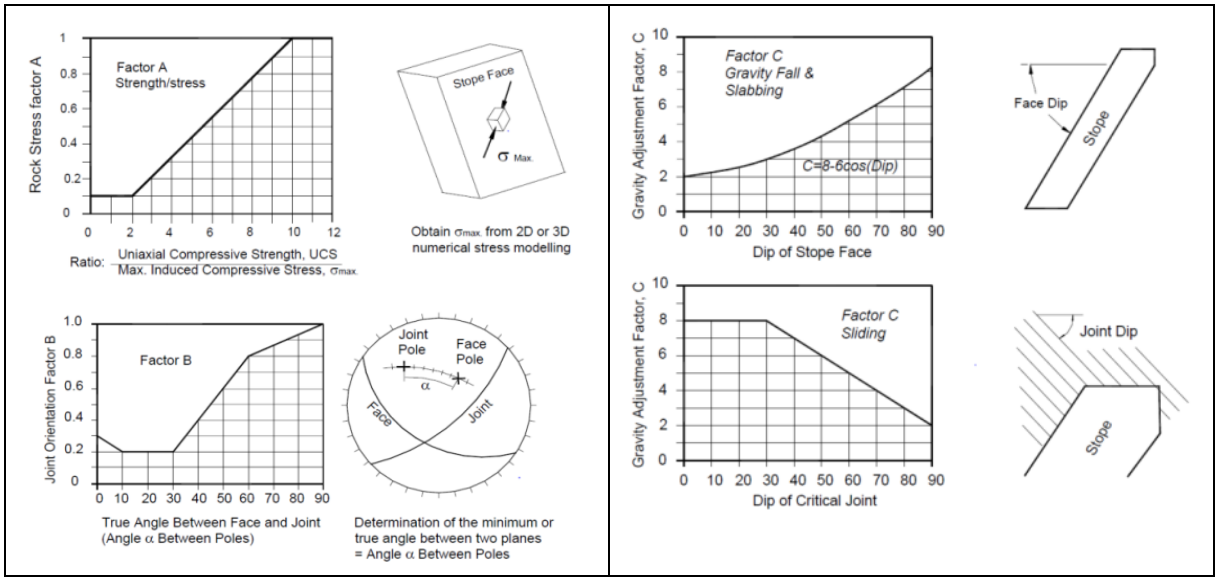

Figure 19 Diagrams to explain how to estimate the Stability Graph Factors A, B and C. After Potvin, 1988, reproduced second-hand from Huchinson and Diederichs, 1996.The 'span' (width or diameter) as used in the Q-system, and the 'span from nearest support' as used in RMR, are replaced by the hydraulic radius, or area divided by perimeter, as commonly used in hydraulics, e.g. HR = XY/(2X + 2Y).

We can note from Figure 18 that in relation to the matrix 'location' for 'caving' and for 'massive failure', both Jn/Jr (as in Figure 17) and Ja alone have quite significant 'unfavourable' positions. So not only tunnel-scale overbreak as in the red sketches in Figure 17, but also the larger-scale yellow J1/J2 mechanism are obviously strongly affected by unfavourable Jn/Jr and Ja values.

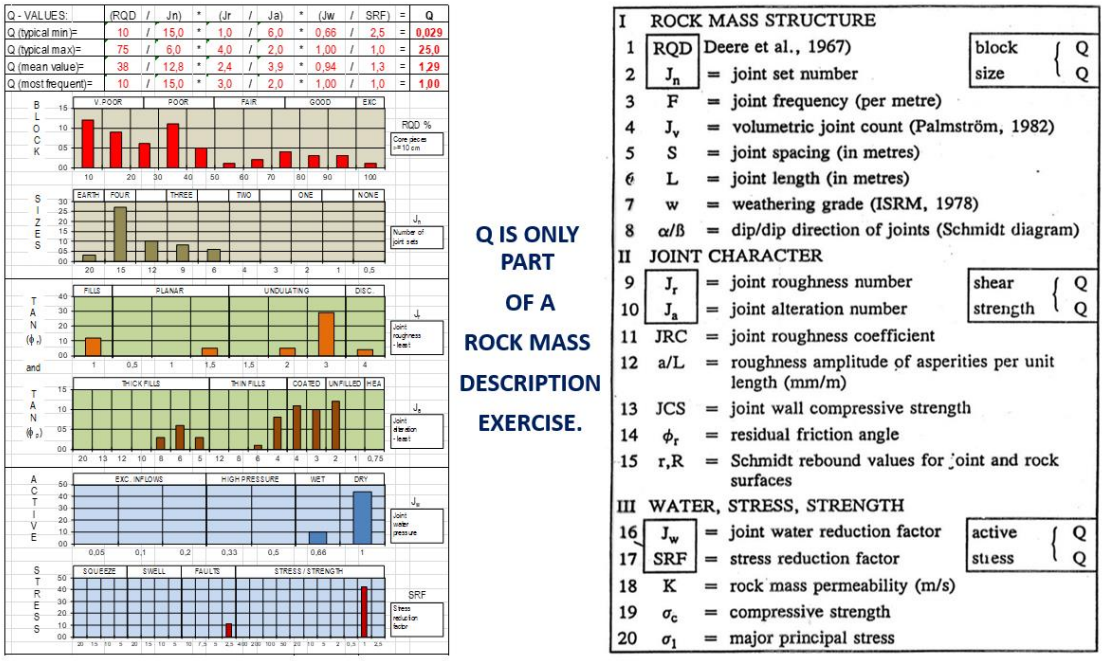

Figure 20 The four Q' parameters that assist with stope dimensioning, and the six Q-parameters (seen as histograms on the left) that are used in characterizing rock masses and tunnelling conditions more fully are obviously just part of the comprehensive data needed for a thorough engineering geological description. Serious consultants do not / should not put a 'blob' on a GSI chart and be satisfied that that is (most of) the required input data for their model. When using the Barton-Bandis model in UDEC-BB, the index tests shown in Figure 21 are utilized, if not relying on the observational judgement of an experienced BB specialist.

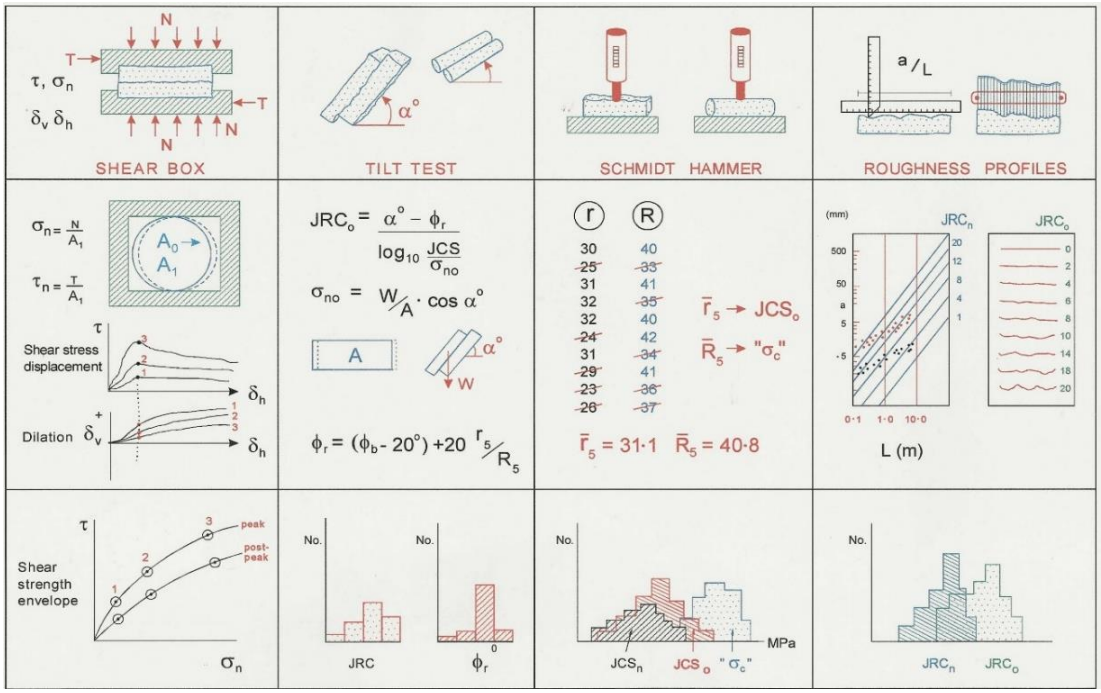

Figure 21 Shear box, tilt test, Schmidt hammer and roughness profiling methods used for evaluating the JRC, JCS and φ_r data for major UDEC-BB modelling projects. In the case of NGI's Sellafield project for UK Nirex (1990-1996) we were logging many kilometers of core and preparing joint samples representing each joint set. Two tunnel models were shown in Figure 10. A large number of deep cavern models were also performed.

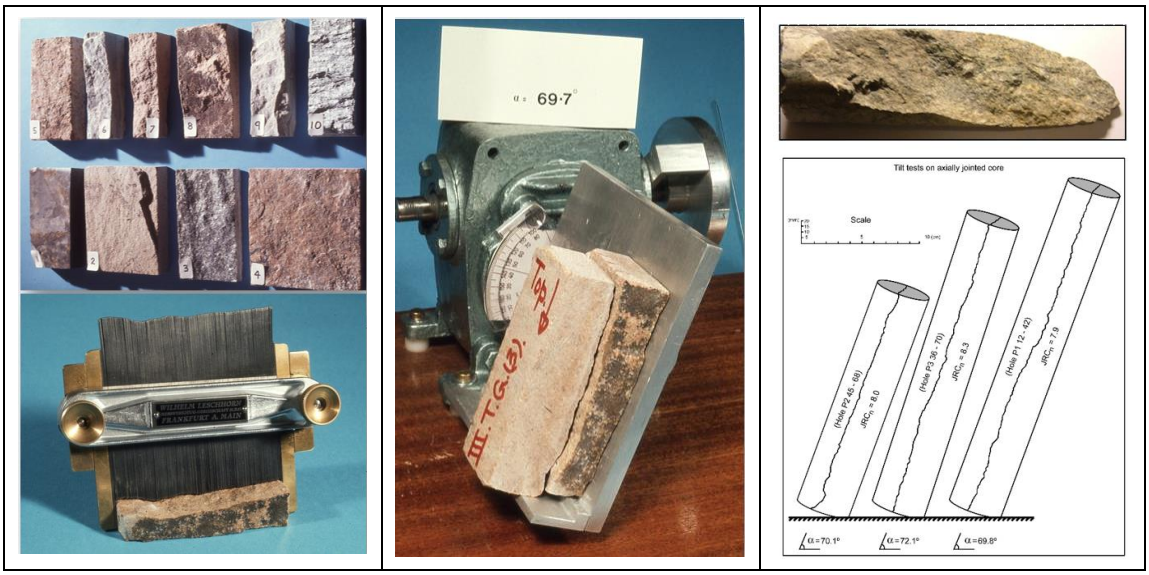

Figure 22 Left: examples of joint profiling and tilt tests. From Barton and Choubey, 1977. Right: samples from TerraTek's heated block test test in Colorado. Barton, 1982.

Three of the most commonly used shear strength criteria for rock joints are illustrated in Figure 23. The classic Mohr-Coulomb involving a cohesion intercept 'c' and a stress-independent friction angle 'φ' was not developed from testing rock joints, which actually do not display actual cohesion intercepts unless very steep (eg. 90º) steps are present in the joint plane, due for instance to cross-joint influence. An improvement for lower stress was suggested by Patton, 1966 with his well-known 'i-values' where 'φ+i' will be the lower-stress estimate. The problem of course is which combination of 'i-values' one should use. This was the impetus for a new student in 1966, and the resulting parameters described above took some years to materialize.

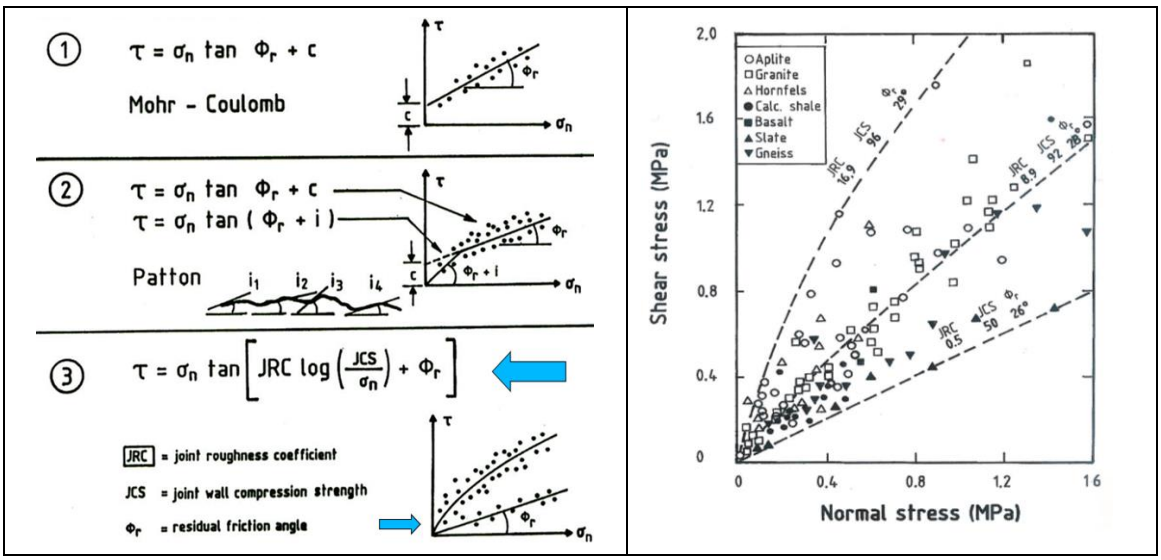

Figure 23 Mohr-Coulomb, Patton (1966) and Barton (1973) shear strength criteria for rock joints. The first version of the JRC, JCS, φ_r criterion was developed from the tension fractures shown in Figure 3: with respective values of 20, UCS and 30º. The direct shear test data shown in the right-hand diagram, from Barton and Choubey, 1977 was confirmation of close predictability of parameters and resulting shear strength, using the index tests (Fig.21). Note that multi-stage shear testing of the same joint sample at increasing normal stress causes rotation of the shear strength envelope. Artificial life support for 'c' and reduced 'φ'.

Interaction between tunnels due to deep EDZ

It is perhaps to be expected that those who favour continuum modelling might claim that the patterns of joint deformation illustrated in Figure 24 could be ‘matched’ with colour codes representing different degrees of ‘plastic behaviour’. However, this can be challenged if using GSI and Hoek-Brown et al equations (to be reviewed shortly), since there is not actually a block-size scale involved in ‘the sketches’, and except in some later attempts at better quantification of GSI, there is no RQD representing the helpful ‘start’ to both RMR and Q. In the Q-system RQD is used directly if RQD ≥ 10.

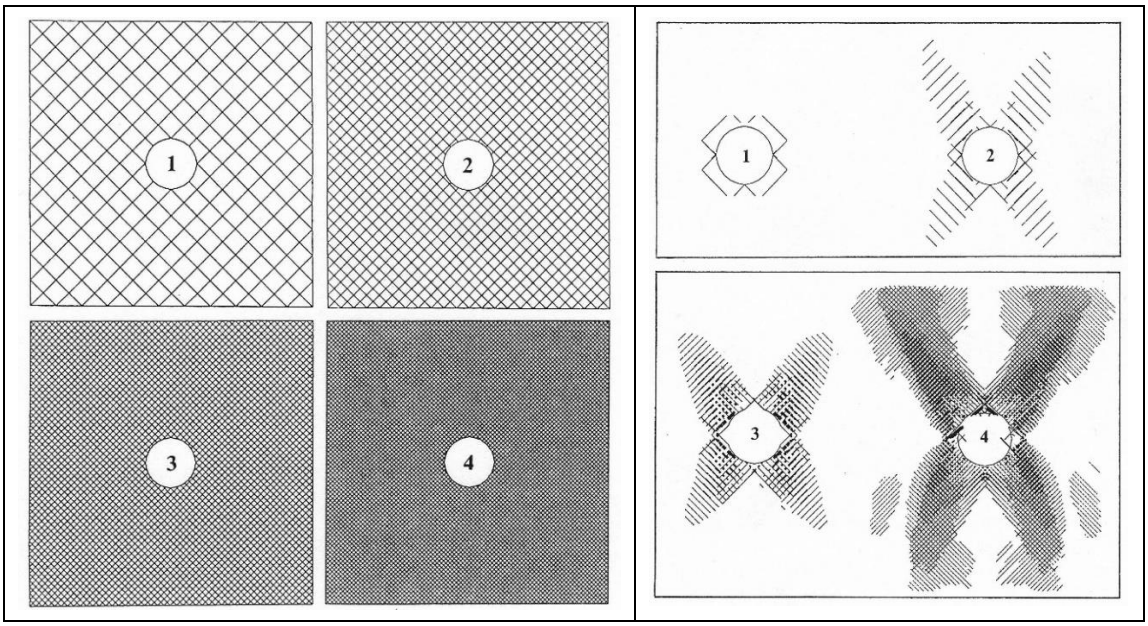

Figure 24 UDEC-MC study of successively halved block size, such that model #4 has 10,000 blocks, suggest good reasons for wider separation of tunnel tubes where there is a risk of crossing major fault zones, with the added threat of clay and small block sizes. Shen and Barton, 1996.

On several occasions the writer has observed the effects of too close tunnel spacing, such as the Pinglin motorway tunnels in eastern Taiwan, where the 5m diameter pilot bore was ‘squeezed’ even by the 13m running tunnel TBM being two diameters distant. The pilot tunnelling was arrested at least 13 times, and a steel-mesh vertically-squashed elliptical ventilation tube for clearance by the train was required.

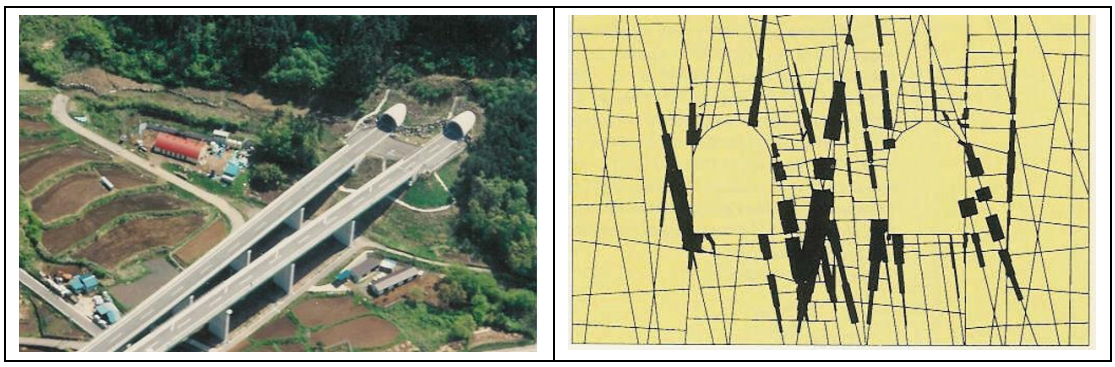

Figure 25 Observation of prudent tunnel spacing from a helicopter ride in Japan. The UDEC-BB model is of the planned cable-anchor concrete-filled caverns for the 2.2km Tsing Ma suspension bridge. Weak cavern-parallel features (see modelled shearing, and see Figure 25) resulted in the choice of 70x70x70m (approx.) gravity anchors for the cables.

Figure 25 Looking parallel to the unavoidable but unfavourable (weak-in-shear) axes of the originally planned cable-anchor caverns for Tsing Ma suspension bridge. Huge loads were planned due to the combined motorway and rail triple-decker box structure.

Where continuum modelling can be the only choice but how to do it?

A suggested scheme for choosing which type of computer modelling is appropriate for which type of rock mass is shown in Figure 26. In the earlier examples of UDEC-BB given in this paper, we were well within the suggested Q-range of 0.1 (very poor) to 100 (very good). It was possible for engineering geologists to suggest a realistic and representative joint pattern, which was digitized so that it could be reproduced as perhaps one of several UDEC model geometries. If the rock mass by comparison is highly fractured as symbolized in the left side of the figure, then a continuum approach may be needed. However, care is needed in assuming that GSI and Hoek-brown equations of assumed rock mass behaviour will give relevant results. There is unfortunately evidence of grossly exaggerated 'plastic zone' prediction, as revealed in an international court case some years ago. This can hardly be due to the commercial FEM method used at that time.

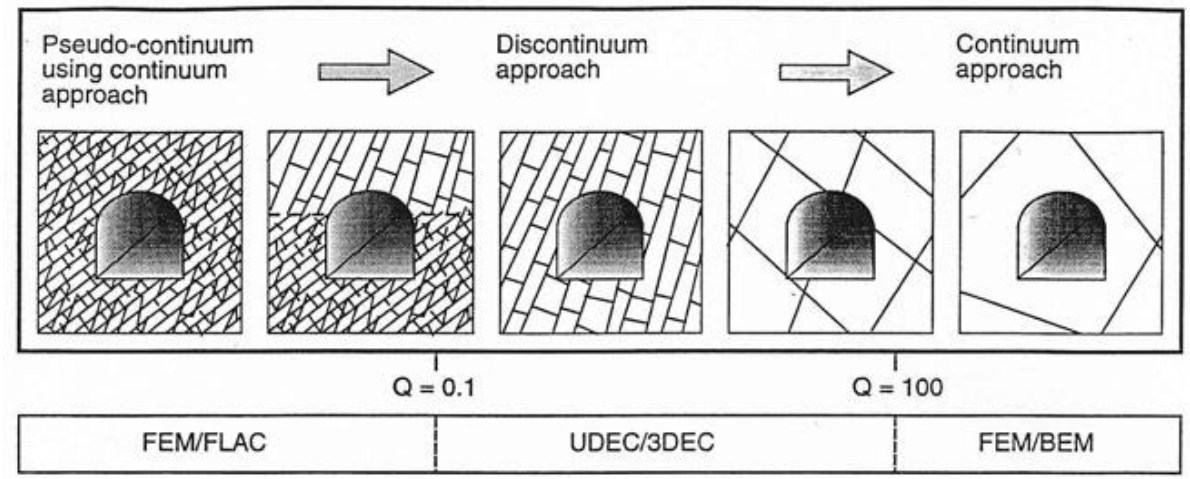

Figure 26 A scheme for helping in the selection of appropriate computer models, based on a 'degree-of-fracturing' scheme with an implied 'central' Q-scale. Logic would suggest this is stretched to 0.01 or worse to the left side, and to an almost unjointed Q = 500 to 1000 on the right side. In Figure 27 a continuum model using FLAC is compared with a UDEC-BB model. In that particular case we are not down at low Q-values as referred to here, so the deformation is small. It would certainly not be small if the deformation modulus (and shear strength) were appropriately low due to low Q-values. (See later Q-modulus relationship).

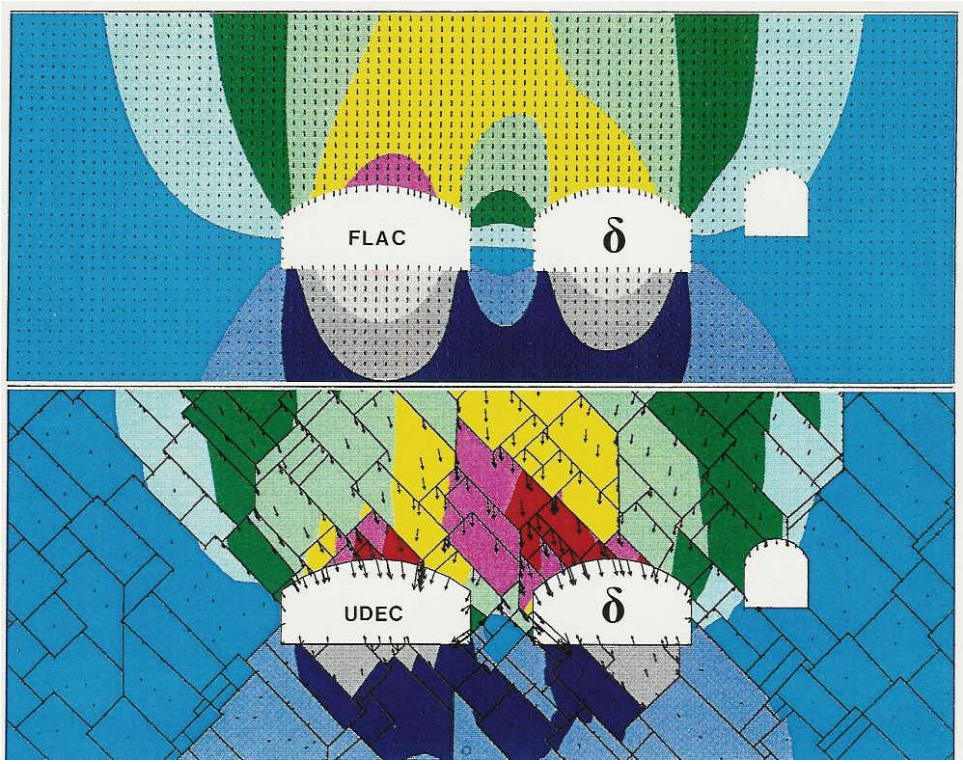

Figure 27 The deliberate modelling by a former NGI colleague Lisa Bacher, of the same triple-tunnel motorway using the same boundary stresses and the same intact-block moduli. The jointing makes the UDEC-BB model 'infinitely' more relevant than the continuum model.

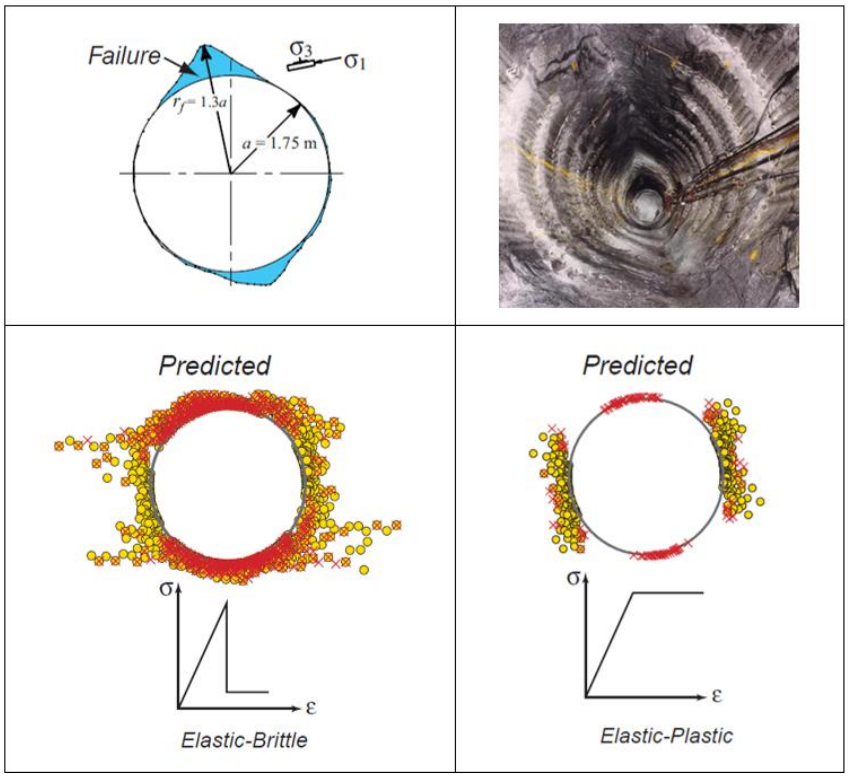

Figure 28 Mohr-Coulomb tri- and bi-linear elastic-brittle and elastic-plastic models of the well-known URL (Manitoba) line-drilled mine-by tunnel. Magnitudes of the input parameters came from GSI and H-B estimation. The objective of the modelling was to show the great improvement that results if the cohesion assumption is degraded while friction is mobilized, as in Figure 29. The M-C results are surprising. Hajiabdolmajid, Martin and Kaiser, 2000.

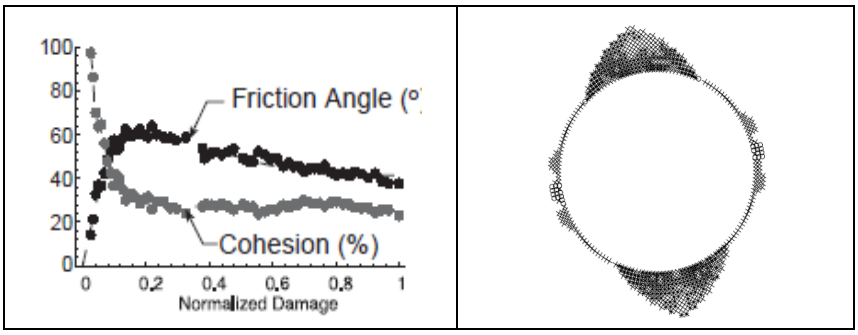

Figure 29 A greatly improved result using a CWFH (cohesion weakening friction hardening) approach. Hajiabdolmajid, Martin and Kaiser, 2000. The writer and a colleague also used this CWFH approach using Q-based input data. See Figure 31.

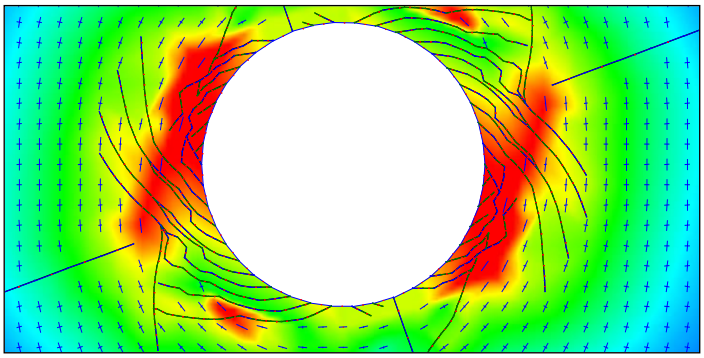

Figure 30 The BEM fracture mechanics code FRACOD developed by Shen et al. 2002, 2013, which shows a realistic development of log-spiral failure surfaces when jointing presence is sparse (the right-hand side of Figure 26). Red represents low, and green represents high factor of safety against further fracturing. In situ stress levels are > 40% of UCS. Priv. comm. Shen 2004. These were scoping studies for the sub-Andean Olmos tunnel where there were rock-burst challenges, since a 'stress-raising' TBM method had to be used in the contract.

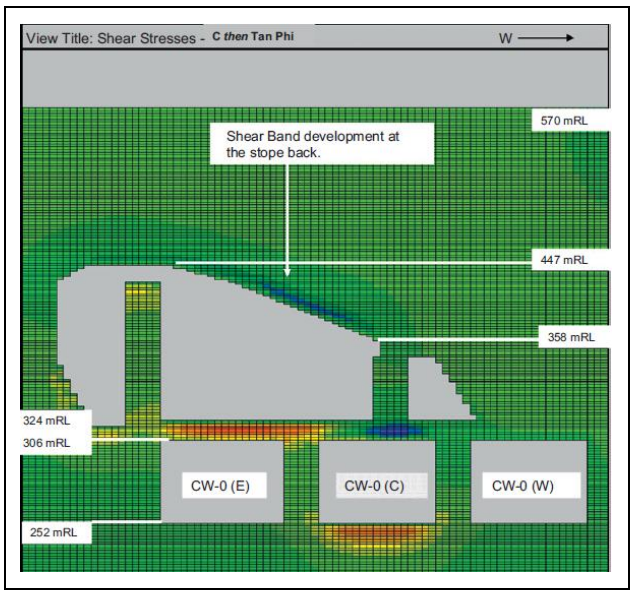

Figure 31 FLAC3D continuum model using 'c then tan φ' (degraded cohesion CC from Q-formula) and mobilized friction FC from Q-formula). Barton and Pandey, 2011. There are encouraging signs that others in the profession are testing this approach and obtaining better matches with observed behaviour. See for instance Edelbro, 2009 who utilized degradation of c and mobilization of φ in Phase 2, one of the FEM programs of Rocscience.

A critique of GSI and Hoek-Brown equations for continuum analyses

In the opinion of the writer it is rather remarkable and somewhat discouraging for the future of our subject 'rock engineering' for civil and mining projects, that so many young (and not so young) people have adopted the Rocscience promoted and of course Hoek promoted GSI, with the associated Hoek-Brown equations (see below).

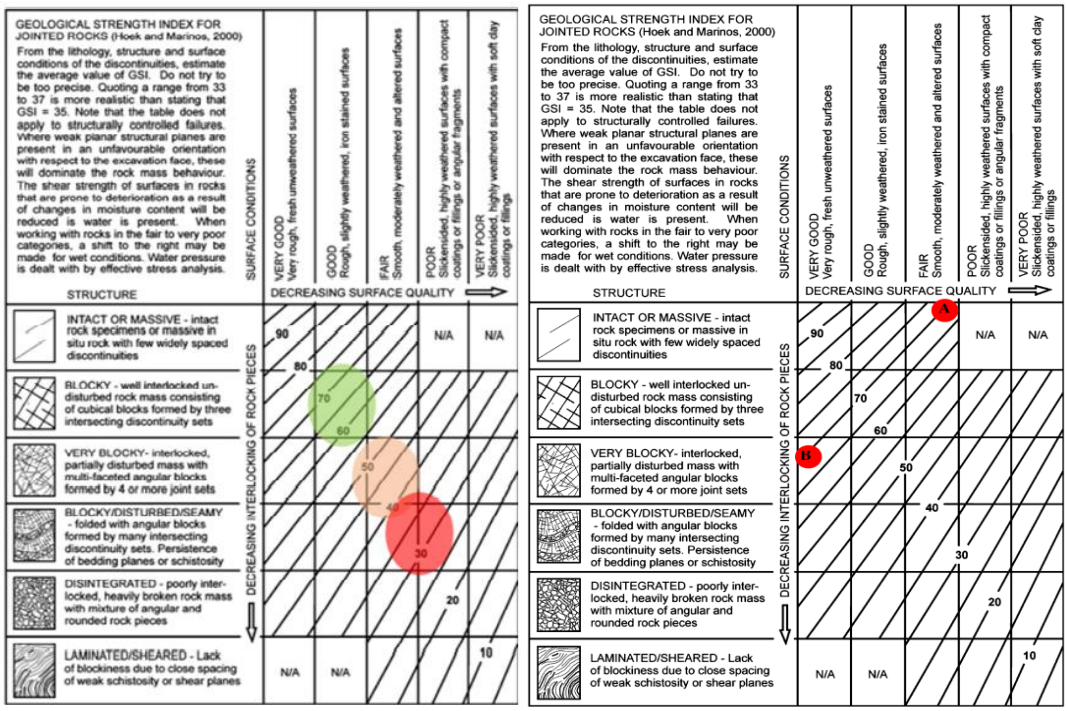

$$C_m = \frac{\sigma_{ci}\left((1+2a)s + (1-a)m_b\sigma_{3n}\right)\left(s + m_b\sigma_{3n}\right)^{a-1}}{(1+a)(2+a)\sqrt{1+\left(6am_b\left(s+m_b\sigma_{3n}\right)^{a-1}\right)/(1+a)(2+a)}}, \quad (1)$$

$$\phi_m = \sin^{-1}\frac{6am_b\left(m_b\sigma_{3n}+s\right)^{a-1}}{2(1+a)(2+a)+6am_b\left(m_b\sigma_{3n}+s\right)^{a-1}}, \quad (2)$$

$$\sigma_{3n} = \frac{0.47\sigma_{cm}^{0.06}(\gamma H)^{0.94}}{\sigma_{ci}}, \quad (3)$$

$$m_b = m_i \exp\frac{\mathrm{GSI}-100}{28-14\,D}, \quad (4)$$

$$\sigma_{cm} = \sigma_{ci}\cdot\frac{\left(m_b+4s-a\left(m_b-8s\right)\right)\left(m_b/4+s\right)^{a-1}}{2(1+a)(2+a)}, \quad (5)$$

$$E_{rm}(MPa) = 100.000\,\frac{1-D/2}{1+e^{(75+25D-GSI)/11}} \quad (6)$$

$$E_{rm}(MPa) = E_i\left(0.02+\frac{1-D/2}{1+e^{(60+15D-GSI)/11}}\right) \quad (7)$$

Figure 32 The GSI selection scheme based on a brief encounter with 'geology' (the sketches) to be followed by what could be called 'food-blender' black-box modelling.

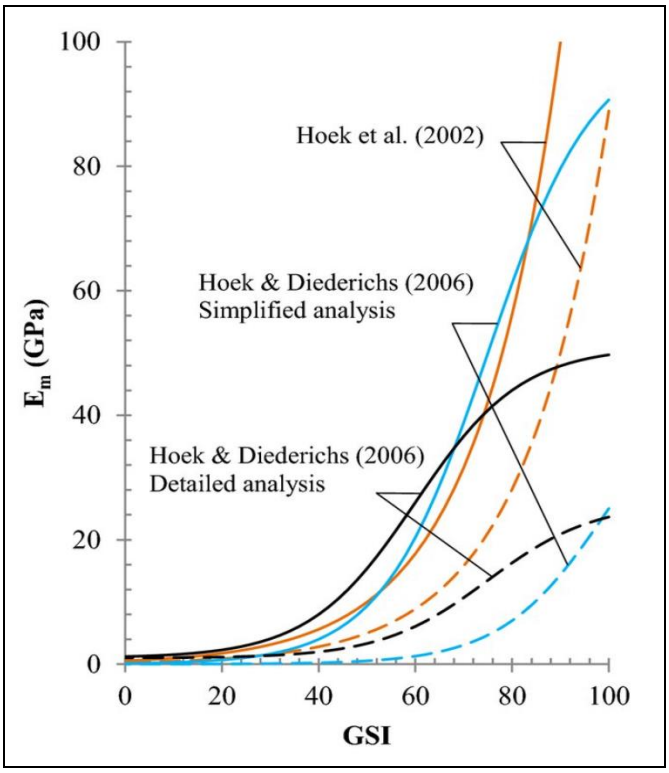

Figure 33 The hopeless deformation modulus advice connected with GSI. From: Renani and Cai, 2021: Forty-Year Review of the Hoek–Brown Failure Criterion for Jointed Rock Masses.

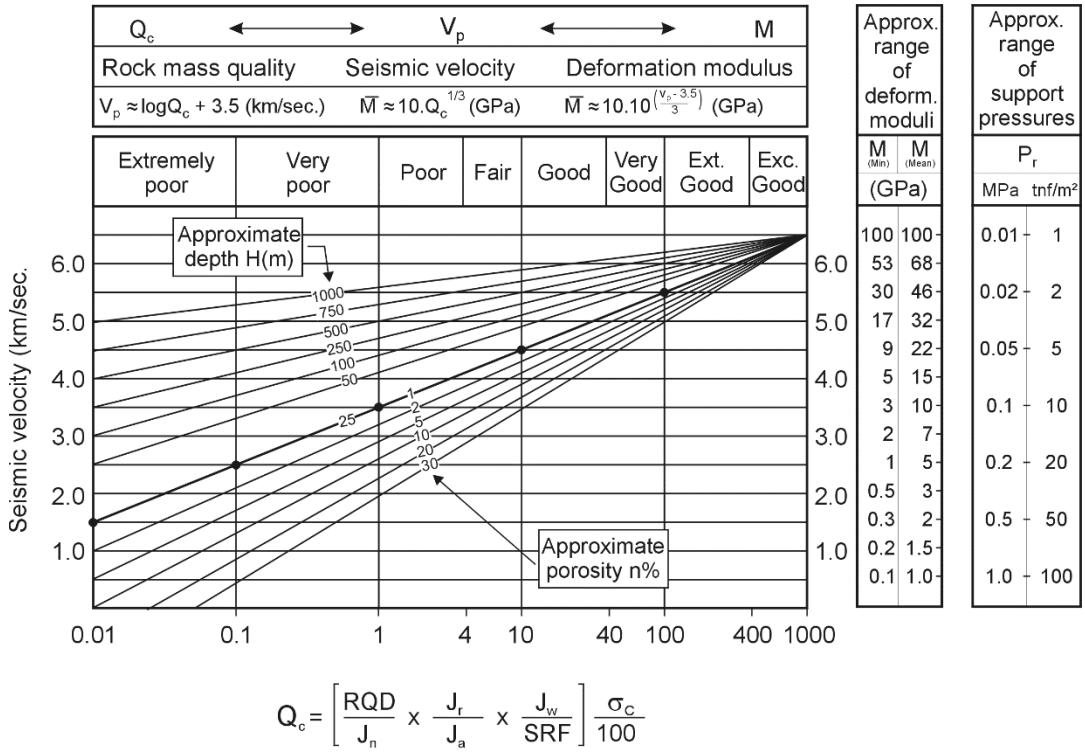

Figure 34 A more scientific alternative for linking rock mass deformation modulus with a rock mass characterization method and cross-checking with the P-wave velocity. The method shows approximate depth (+ve) and porosity (-ve) correction. From Barton, 1995, 2002. Note that as an approximation E_{mass} (or M) ≈ $10^{(Vp - 2.5 + \log \sigma c)/3}$, from Barton, 2007.

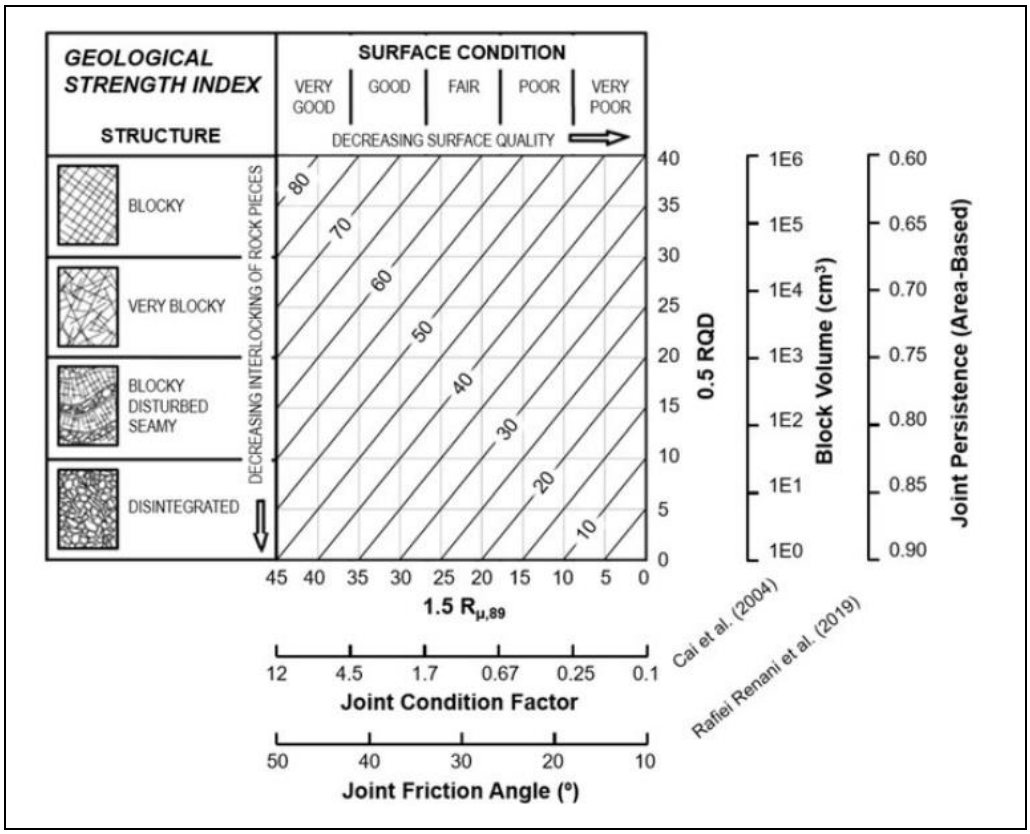

Figure 35 Particularly creative additions for 'better' quantifying GSI. Renani and Cai, 2021.The better-known methods are listed in Table 1. It is a somewhat surprising list.

Table 1 A selection of some equations used to improve the quantification of GSI. Why a published method should require so much improvement is not clear. Ván & Vásárhelyi, 2014.

$GSI1 = RMR - 5 = R1+R2+R3+R4+R5(=15) - 5$	(1)
$GSI2 = 1.5\ R4 + 0.5\ RQD$	(2)
$GSI_3 = 15 \log\left(\frac{RQD}{Jn}\frac{Jr}{Ja}\right) + 50$	(3)
$GSI_4 = 9 \ln\left(\frac{RQD}{Jn}\frac{Jr}{Ja}\right) + 44$	(4)
$GSI_5 = \frac{52Jr/Ja}{(1+Jr/Ja)} + 0{,}5RQD$	(5)
$GSI_6 = \frac{26{,}5 + 8{,}79\ln Jc + 0{,}9\ln Vb}{1 + 0{,}0151\ln Jc - 0{,}0253\ln Vb}$	(6)
$GSI_7 = 153 - \frac{165}{\left[1+\left(\frac{Jp}{0{,}19}\right)^{0{,}44}\right]}$	(7)

Some examples of slope stability: real, discontinuum, continuum

With the exception of highly-trafficked road-cuttings and railway-cuttings, and urban slopes above pavements, and of course some critical high-dam valley slopes, there will generally not be any thought of bolting or cable anchors for ensuring rock stability in general. There are millions and millions of rock cuttings. Temporary and more permanent open-pit mine slopes suffer the same no-bolting fate for obvious economic reasons. So, since there may be no rock bolts, the selection of stable slope angles will often have to depend on the properties of the local jointed rock including joint orientations. This is the philosophy behind Q_{slope} (Barton and Bar, 2015). Design-chart case records mostly collected by Bar are shown later. (Bar and Barton, 2017).

Figure 36 The importance of photographs of real rock slopes, showing some details that will never be captured adequately in continuum modelling. Top: Eidfjord, S W Norway. Photo N. Barton, 1971. Bottom: rail bridge access road, Northern Railways, Indian Kashmir, 2009.

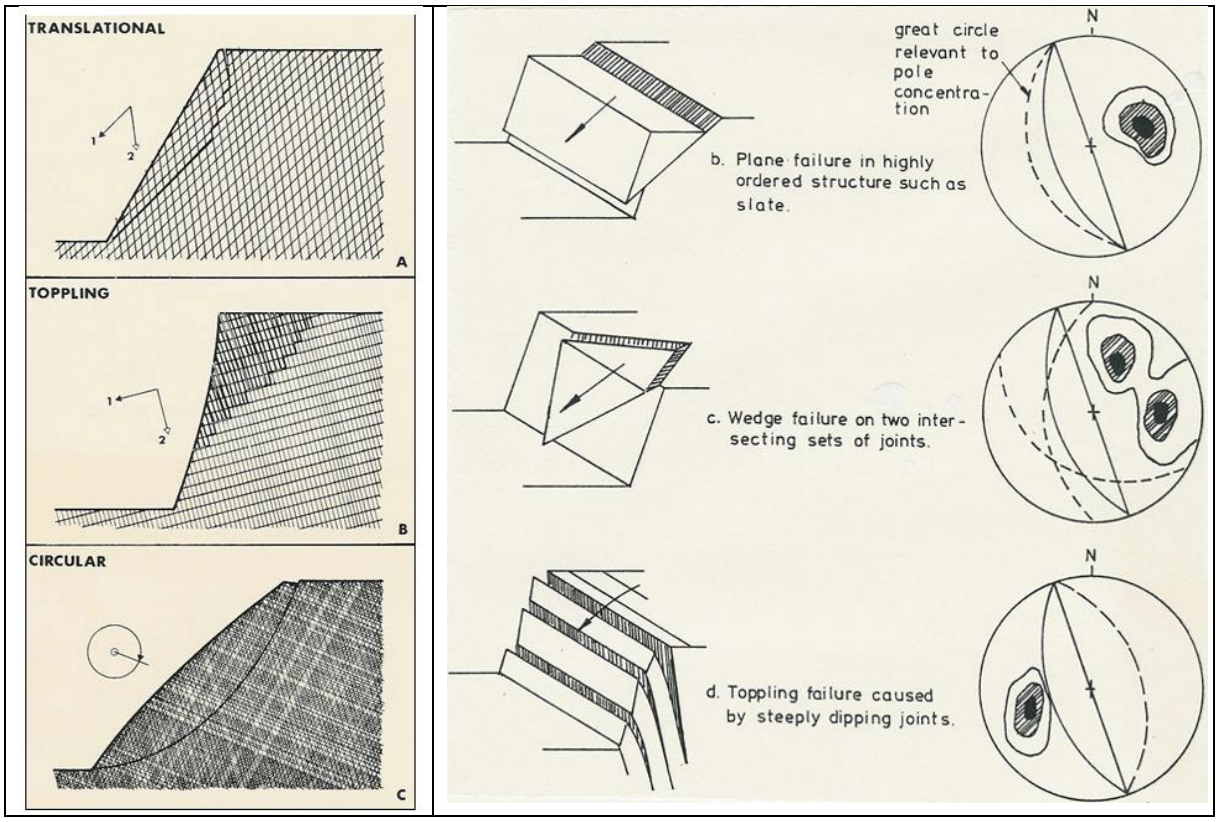

Figure 37 Left: three basic modes of instability from Barton, 1973. Right: Hoek and Bray, 1974 wedges and stereographic lower-hemisphere friction angle - slope angle assessments. Note that the bulking drawn in the lower-left 'circular' case was inspired by observations of 'sloughing' within the slopes of an old open-pit with disintegrating slates. The writer collected slope-height slope-angle data in this and nearby Rio Tinto pits, in southern Spain, 1968-69.

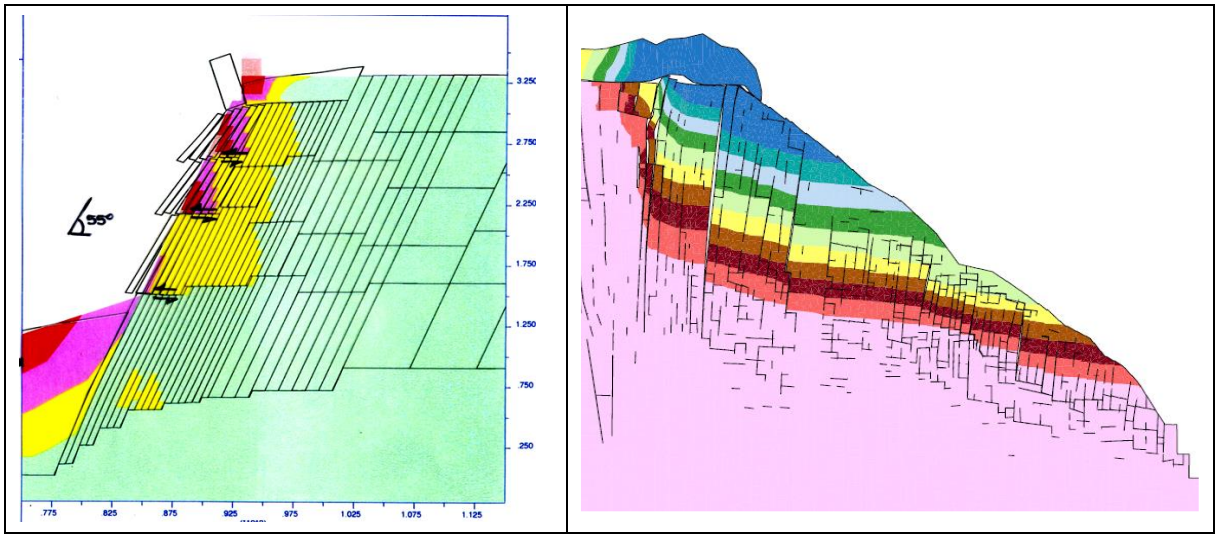

Figure 38 Some unconventional UDEC modelling by Bandis. Left: investigating the stability of the slopes below the Castle of Mytilini. These are in the book by Barton and Bandis, (in preparation). Obviously, the abilities of slower discontinuum modelling are far removed from the serious 'geological' limitations of the much faster continuum modelling.

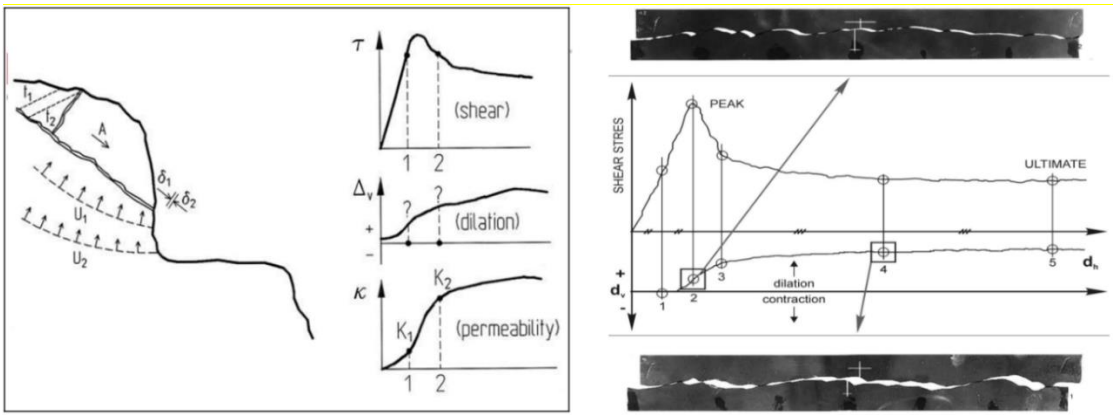

Figure 39 Some of the fundamentals of slope stability when (because) joints are so often involved. Right-hand shear-test reconstructions of the measured dilation paths, from Barton, 1971, 1973.

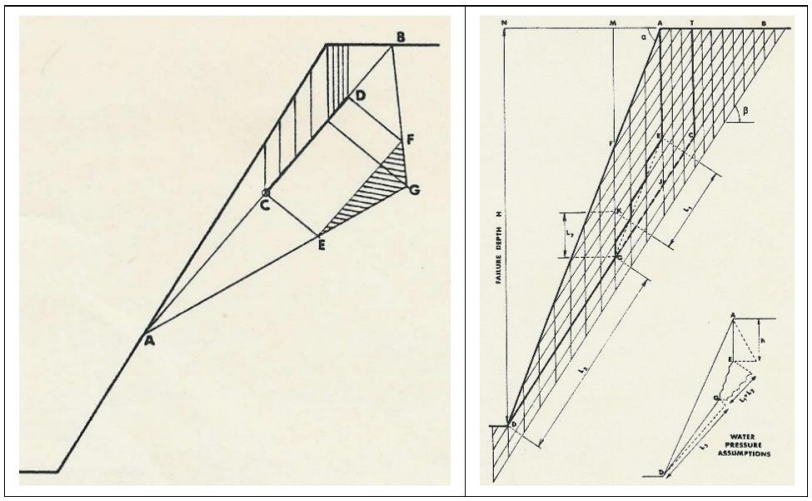

Figure 40 Possible reasons for stepped (and 'internal') failure surfaces are the sub-crest maximum shear stress and progressive accumulation of shear displacement. Barton, 1971.

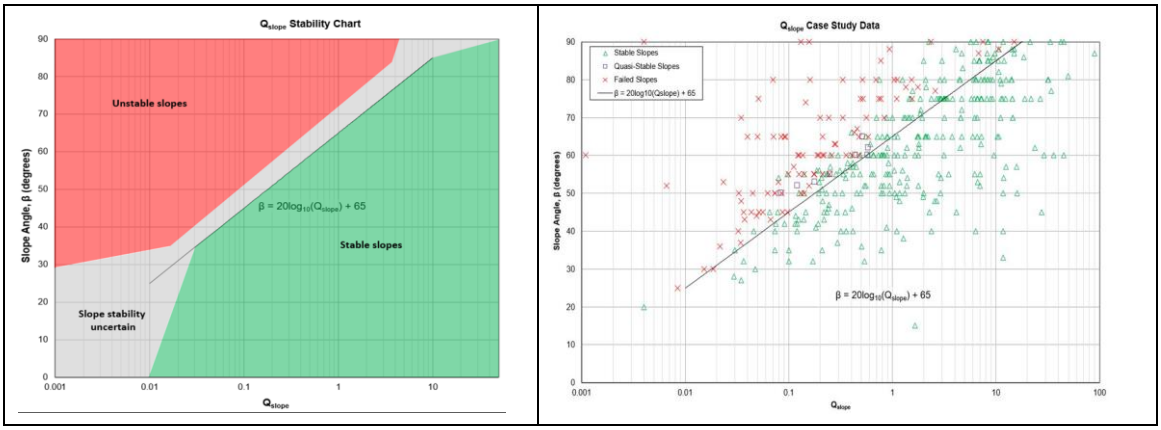

Figure 41 The Q_{slope} method is based on Q with almost unchanged RQD, Jn, Jr and Ja but wedge stability is considered so pairs of Jr/Ja apply to different sides of potential wedges, with relevant weightings. Since slopes are under lower stress than many tunnels SRF has three appropriate categories, and Jw is now called J_{wice}. Tropical rain and ice-wedging can be roughly assessed. The method was developed by the writer, but co-author Neil Bar has been a very active collector of case records. Barton and Bar, 2015, Bar and Barton, 2017.

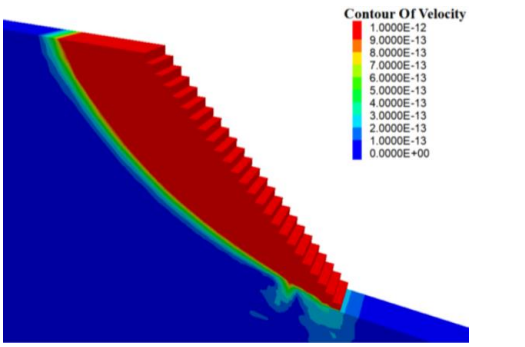

Parameter		Rock Mass B
Density	ρ (t/m^3)	2.7
Intact Young's Modulus	E_i (GPa)	28.2
Geological Strength Index	GSI	40
Hoek Brown Constant	m_i	10
Intact uniaxial compressive strength	UCS (MPa)	20

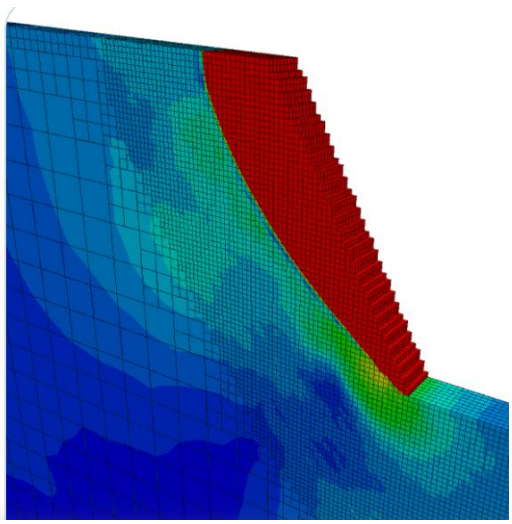

Figure 42 Continuum modelling contrasts. Left: 3DEC slice of a 200m high open-pit slope, using the IUCM constitutive model. Such spoon-shaped failure is possible in rockfill and in soil, but the writer does not believe it has been seen in competent jointed rock. Styles and Vakili, 2020.

According to the above authors, the recently developed '*Improved Unified Constitutive Model' (IUCM) takes the best parts of Mohr-Coulomb and Hoek-Brown, with integrated confinement-controlled softening/hardening of cohesion and friction, confinement-controlled changes in the dilation angle, and porosity-controlled modulus softening'.* For some reason presumably connected with the errors in Hoek-Brown, giving incorrect c and φ, the end result is something only seen in rockfill or soil. It apparently has a limited actual relation to geology or jointed/faulted rock.

The circular failure beliefs of Mohr-Coulomb and Hoek-Brown aficionados, with Carranza-Torres, 2021 a chief contributor and probably largely responsible for the smooth curves of the H-B rockmass criterion of 2002 (and the associated remarkably complex equations) has given a very detailed recent treatise. Figure 43 is his clear but apparently misleading introduction, as it does not correspond to competent rock.

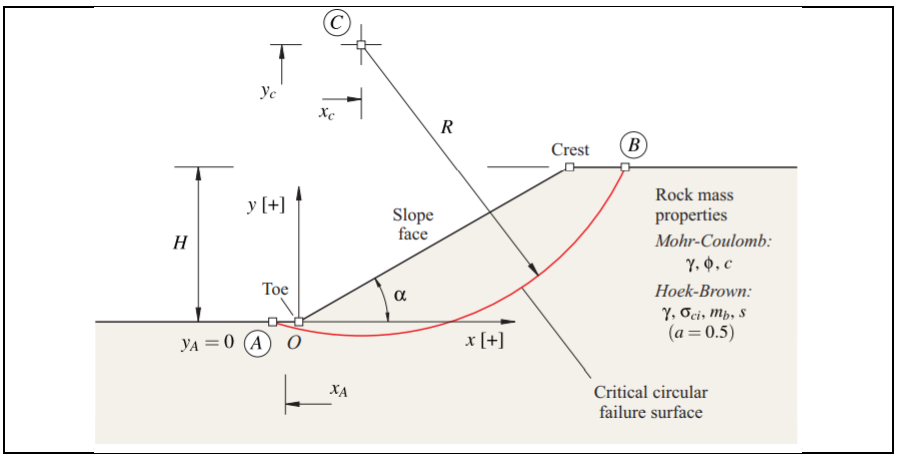

Figure 43 According to Carranza-Torres, 2021 this figure represents <u>'a section of a rock slope in a rock mass that obeys the Mohr-Coulomb or Hoek-Brown failure criteria'.</u> In the opinion of the writer, this is a perfect description of the errors in 'rock mechanics' seen during the last 50 years since Müller in 1966 and Brace even earlier warned not to add 'c' and 'φ'.

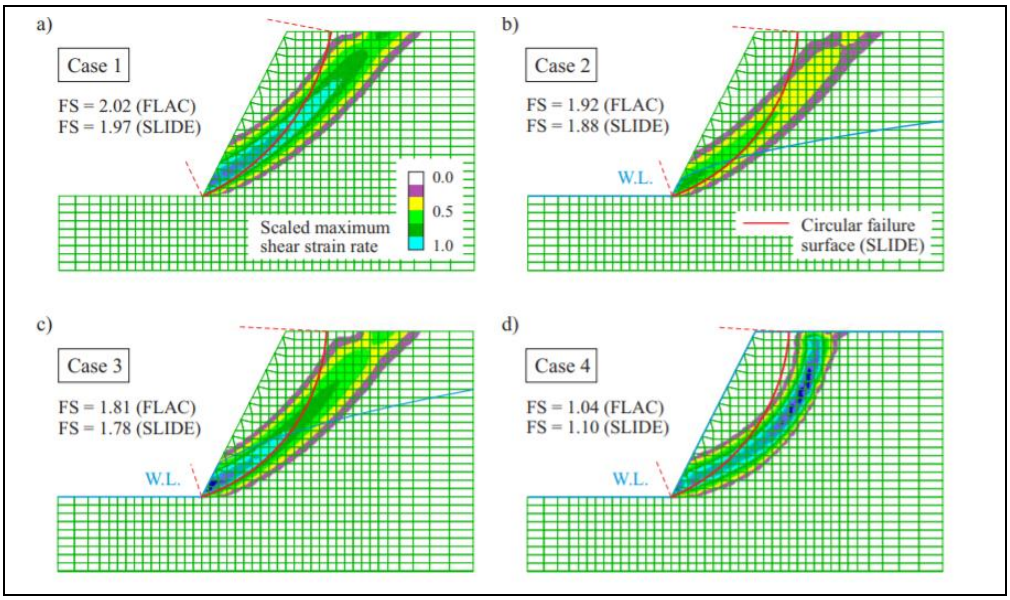

Figure 44 Further 'circular' failure analyses using both FLAC and SLIDE computer modelling, apparently with input of c and φ derived from a combined GSI and Hoek-Brown. Carranza-Torres, 2021. These are basically resembling failure in soil, and only apply to very weak rock.

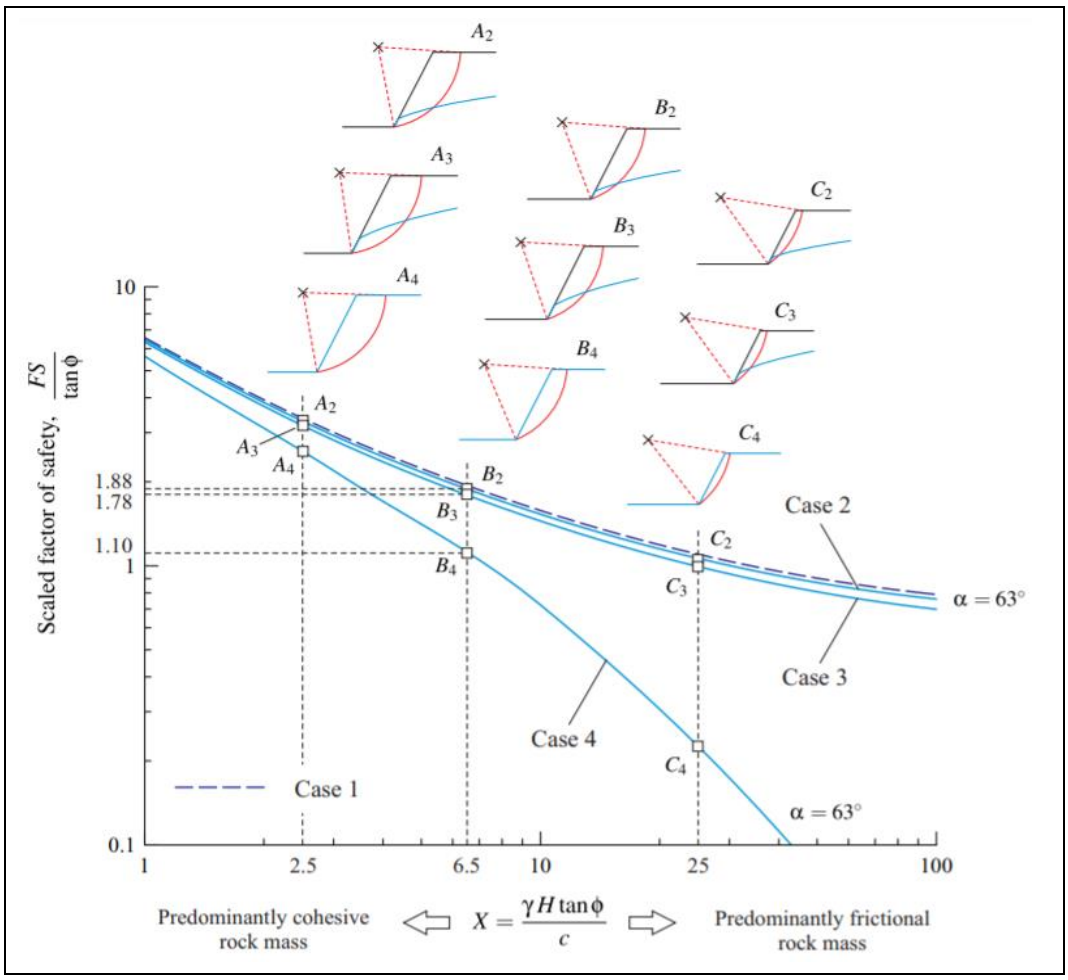

Figure 45 The 'elegance' of the relative 'c' or 'φ' dominance given by Carranza-Torres, 2021 in his many impressive 'design charts' cannot be denied. The relevant depths of the various spoon-shaped predicted failures are interesting. But they do not apply to jointed rock.

Carranza-Torres, 2021 has revealed his belief, backed up by reference to the four following pit-slope failures in the following opinion. '*In all cases, due to the scale of the failure, the rock mass fails resembling typical circular (or rotational) failures observed in failed slopes in soils —even when the collapsed rock mass (or rock fill) may be comprised of rock blocks of the size of a truck!'* He is of course correct about the soil-like appearances but is neglecting that unless the rock is very weak, the appearance of 'soil' is actually due to the relative minute scale of rock blocks compared to run-out distance, which is up to 3 km in the case of d) in Figure 46.

As we shall see d) has been misinterpreted by many authors as evidence of 'circular failure'. It is actually fault-plane dominated, as so often in major open-pit failures, that also mobilize and overcome the shear strength of rock bridges and suitably oriented joint sets. These are not 'Mohr-Coulomb' or 'Hoek-Brown' materials. In the future we might use the synthetic rock mass approach of Mas Ivars, Pierce and co-authors including Cundall (2011). However, demanding computing when using basically a 'jointed PFC' approach is not attractive at a large scale, but is definitely interesting for investigating scale effects in jointed 'samples' of very large 'in situ' test scale.

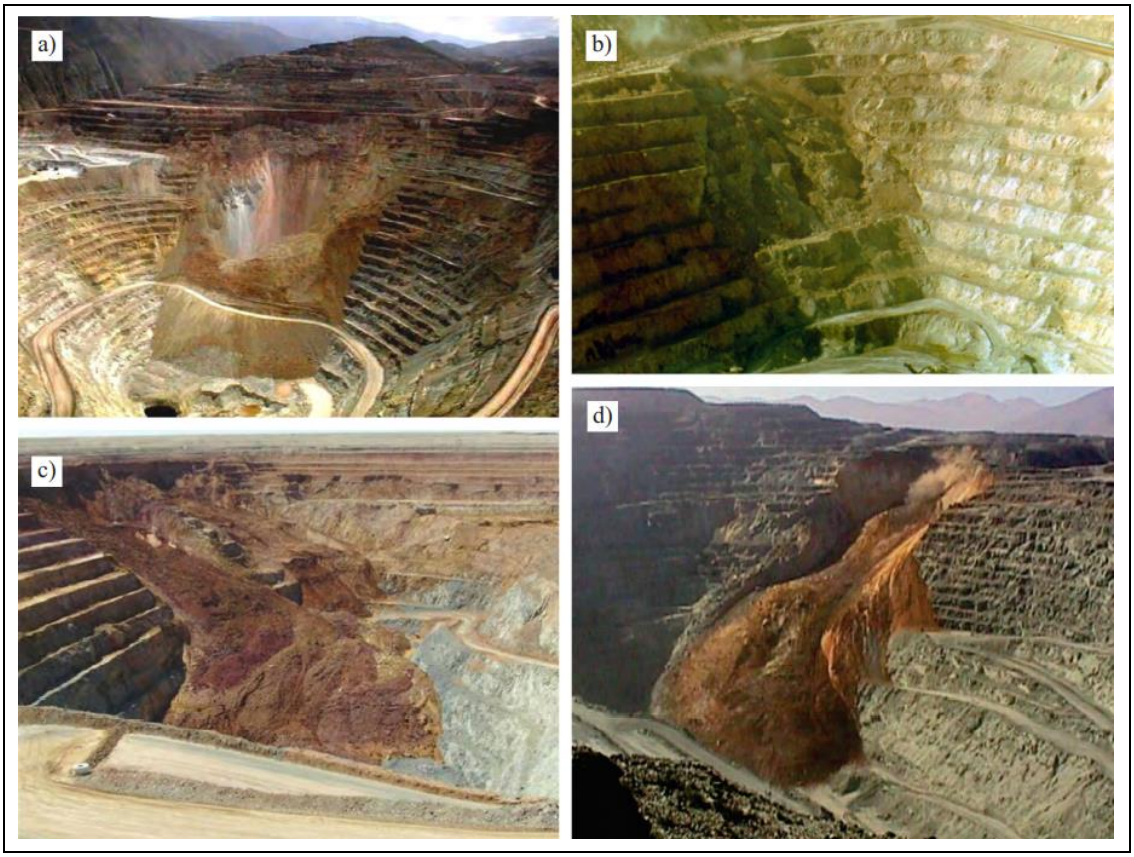

Figure 46 The four major open-pit failures reproduced from others by Carranza-Torres, 2021 are reproduced again by the writer, but for different reasons. Cases a) and b) are strictly 'internal' failures that do not extend beyond the crest of the slopes.

Case c) in the above figure is actually *lake-bed sediments and saprolite*, hardly of relevance to jointed rock or rock masses. Martin and Stacey, 2013 give a nice analysis of the behaviour of such weak materials, also citing classic soil mechanics literature. Case d) measures 3km from crest to toe and actually involves failure of an unconfined nose at the crest and shearing down a long (0.5km(?) fault plane. It does not involve soil, nor is it a 'circular' failure example as assumed by Carranza-Torres.

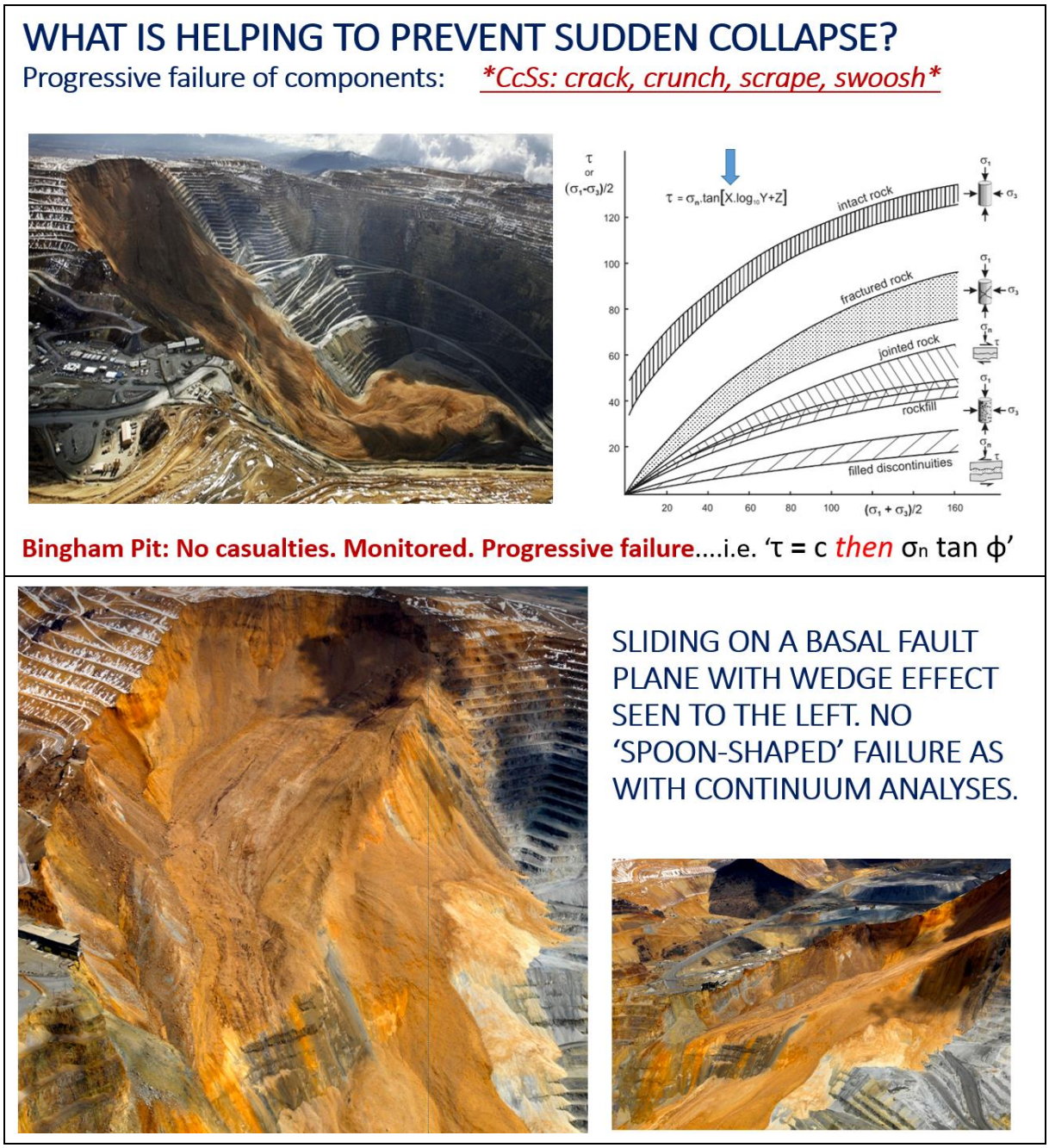

Figure 47 These are two recent conference PP (N. Barton, 2021 'Continuum or Discontinuum – GSI or JRC??). The photos emphasise the error in numerous papers describing this pit failure. A preliminary suggestion of degrading 'c' and then mobilizing the frictional component, as done by Hajiabdolmajid, Martin and Kaiser, 2000 and Edelbro, 2009 and Barton and Pandey, 2001 is made. However, attention is directed to the four potential components CcSs as a future solution to progressive failure. Barton, 1999. (See Appendix).

Conclusions

1. In this lecture the writer has attempted to put back jointing and geology into the practice of rock mechanics modelling and understanding. Following the limitations but useful lessons from physical fracture models, a number of UDEC-BB models are reproduced to emphasise the possibility of representing 'geology and structure' at least in 2D and occasionally in 3DEC.

2. GSI with the ‘G’ in its initials has actually removed the geology from our subject, once users leave the six ‘sketches’ and progress to the Hoek-Brown equations and Rocscience software and the impressive curves of shear strength. Regrettably the uniquely opaque ‘black-box’ analyses effectively become homogenized as in a food blender. Continuum behaviour is clearly misleading many and is hardly rock engineering or rock mechanics.

3. We have been warned for more than 5 decades – historians in our subject would claim even longer – that we should not add ‘c’ and the frictional component of strength based on ‘φ’ ($\sigma_n \tan \varphi$). At the very least it should be *‘c then sigma n tan phi’.* This separation in time and deformation is logical.

4. A newer proposal for a more comprehensive (progressive) failure criterion is the CcSs *‘crack’ ‘crunch’ ‘scrape’ ‘swoosh’* suggestion of Barton, 2020. This has the ability to add the progressive contributions of the broken cohesion of rock bridges, the resulting rough, fresh fracture surfaces, the joints (if one or more sets are suitably oriented, and finally the lower resistance of faults of clay-filled discontinuities. (See Appendix for larger scale version).

References (the authors progressive understanding is reflected in many NB refs)

Bandis, S. C., Lumsden, A. & Barton, N. 1981. Experimental studies of scale effects on the shear behaviour of rock joints. Int. J. of Rock Mech. Min. Sci. and Geomech. Abstr. 18, 1-21.

Bandis, S. C., Lumsden, A.C. & Barton, N. 1983. Fundamentals of rock joint deformation. Int. J. Rock Mech. Min. Sci. and Geomech. Abstr. Vol. 20: 6: 249-268.

Bar, N. and N. Barton, 2017. The Q-slope method for rock slope engineering. Rock Mechanics and Rock Engineering. Springer (2017) 50: 3307-3322.

Barton, N. 1971. *A model study of the behaviour of steep excavated rock slopes. Ph.D. Thesis*, Univ. of London.

Barton, N. 1971. Progressive failure of excavated rock slopes. 13th US Symp. of Rock Mech. Stability of rock slopes, Illinois, pp. 139-170.

Barton, N. 1973. Review of a new shear strength criterion for rock joints, Engineering Geology, Elsevier, Amsterdam, Vol. 7, pp. 287-332. Also NGI Publ. 105, 1974.

Barton, N., Lien, R. & Lunde, J. 1974. Engineering classification of rock masses for the design of tunnel support. Rock Mechanics. 6: 4: 189-236.

Barton, N., Lien, R. & Lunde, J. 1977. Estimation of support requirements for underground excavations. Proc. of 16th Symp. on Design Methods in Rock Mechanics, Minnesota, 1975. pp. 163-177. ASCE, NY. Discussion pp. 234-241.

Barton, N. & Hansteen, H. 1979. Very large span openings at shallow depth: Deformation magnitudes from jointed models and F.E. analysis. 4th RETC; Atlanta Georgia, Vol. 2: 1131-1353. Eds Maevis and Hustrulid. Am. Inst. of Min. &, Metall., and Petr. Engrs, Inc. New York.

Barton, N. 1982. Modelling rock joint behaviour from in situ block tests: Implications for nuclear waste repository design. Office of Nuclear Waste Isolation, Columbus, OH, 96 p., ONWI-308, September 1982.

Barton, N., Bandis, S. & Bakhtar, K. 1985. Strength, deformation and conductivity coupling of rock joints. Int. J. Rock Mech. & Min. Sci. & Geomech. Abstr. 22: 3: 121-140.

Barton, N. 1986. Deformation phenomena in jointed rock. 8th Laurits Bjerrum Memorial Lecture, Oslo. Publ. in Geotechnique, Vol. 36: 2: 147-167.

Barton, N., By, T.L., Chryssanthakis, P., Tunbridge, L., Kristiansen, J., Løset, F., Bhasin, R.K., Westerdahl, H. & Vik, G. 1994. Predicted and measured performance of the 62m span Norwegian Olympic Ice Hockey Cavern at Gjøvik. Int. J. Rock Mech, Min. Sci. & Geomech. Abstr. 31:6: 617-641. Pergamon.

Barton, N. 1995. The influence of joint properties in modelling jointed rock masses. Keynote Lecture, 8th ISRM Congress, Tokyo, 3: 1023-1032, Balkema, Rotterdam.

Barton, N. 1999. General report concerning some 20th Century lessons and 21st Century challenges in applied rock mechanics, safety and control of the environment. Proc. of 9th ISRM Congress, Paris, 3: 1659-1679, Balkema, Netherlands.

Barton, N. 2002. Some new Q-value correlations to assist in site characterization and tunnel design. Int. J. Rock Mech. & Min. Sci. Vol. 39/2:185-216.

Barton, N. 2006. *Rock Quality, Seismic Velocity, Attenuation and Anisotropy.* Taylor & Francis, UK & Netherlands, 729 p.

Barton, N. 2007. Near-surface gradients of rock quality, deformation modulus, Vp and Qp to 1km depth. First Break, *EAGE*,October, 2007, Vol. 25, 53-60.

Barton N. 2011. From empiricism, through theory, to problem solving in rock engineering. ISRM Cong., Beijing. 6th Müller Lecture. Proceedings, Harmonising Rock Engineering and the Environment, (Qian & Zhou ed), Beijing Taylor & Francis, (1):3-14.

Barton, N. and S.K. Pandey, 2011. Numerical modelling of two stoping methods in two Indian mines using degradation of c and mobilization of φ based on Q-parameters. *Int. J. Rock Mech. & Min. Sci.,* 48,7: 1095-1112.

Barton, N. 2013. Shear strength criteria for rock, rock joints, rockfill and rock masses: problems and some solutions. J. of Rock Mech. & Geotech. Engr., Wuhan, Elsevier 5(2013) 249-261.

Barton N and N. Bar. 2015. Introducing the Q-slope method and its intended use within civil and mining engineering projects. In Schubert & Kluckner (ed.), Future Development of Rock Mechanics; Proc. ISRM symp. Eurock 2015 & 64th Geomechanics Colloquium, Salzburg: 157-162.

Barton, N.R. and S.C. Bandis, 2017. Characterization and modelling of the shear strength, stiffness and hydraulic behaviour of rock joints for engineering purposes. Rock Mechanics and Engineering, Ed. Xia-Ting Feng, Vol. 1, Principles. Ch. 1, 3-40. Taylor & Francis.

Barton, N. 2020. Unconventional exploration of failure modes in rock and rock masses. Eurock2020, Trondheim (planned but not held due to C19). See Research Gate, 14p.

Barton, N. 2020. Barton, N. 2006. *Rock Quality, Seismic Velocity, Attenuation and Anisotropy.* Taylor & Francis, UK & Netherlands, 729 p.

Tunnelling and Underground Space Technology, Vol. 99, May 2020.

Barton, N. 2021. Details related to ‘the ten’ JRC profiles and further work with the Barton-Bandis criterion – why JRC, JCS and φr. Research Gate. 29p.

Barton, N. 2021. New ideas about failure modes in rock masses – from tunnels to Prekestolen to El Capitan to Everest. Bergmekanikkdag, Oslo. 33.1-33.20.

Barton, N. 2021. Continuum or discontinuum – GSI or JRC?? Keynote lecture. Geotechnical Challenges in Mining, Tunnelling and Underground Structures (ICGCMTU2021) Malaysia. (Research Gate). 39p Screens and lecture.

Barton, N. and S. C. Bandis, 2023. *Engineering in jointed rock.* (Text book in preparation).

Bieniawski Z.T. 1989. Engineering Rock Mass Classifications: A Complete Manual for Engineers and Geologists in Mining, Civil, and Petroleum Engineering, New York, Wiley, 272p.

Carranza-Torres, C. 2021. Computational tools for the analysis of circular failure of rock slopes. Keynote Lecture. In Proceedings of EUROCK 2021. Mechanics and Rock Engineering from theory to practice. Turin. Italy.

Edelbro C. 2009. Numerical modelling of observed fallouts in hard rock masses using an instantaneous cohesion-softening friction-hardening model. Tunnelling & Under-ground Space Tech, 24 (4): 398–409.

Hajiabdolmajid,V., C. D. Martin and P. K. Kaiser, 2000. Modelling brittle failure. *Proc. 4th North American Rock Mechanics Symposium, NARMS 2000* Seattle, J. Girard, M. Liebman, C. Breeds and T. Doe (Eds), 991–998. Balkema.

Hoek. E. and J. Bray, 1974. *Rock slope engineering*. Institute of Mining.

Hutchinson, D.J. and Diederichs, M.S. 1996. *Cable-bolting in underground mines*. BiTech. Publishers Ltd.

Martin, C. D. and P. F. Stacey, 2013. Pit slopes in weathered and weak rocks. Slope Stability 2013. Brisbane. P. M. Dight (ed), Australian Centre for Geomechanics, Perth, 29p.

Mas Ivars, D., M. E. Pierce, C. Darcel, J. Reyes-Montes, D. O. Potyondy, R. P. Young and P. A. Cundall, 2011. The synthetic rock mass approach for jointed rock mass modelling. Int. Jour. of Rock Mech. & Min. Sci. 48 (2011) 219–244

Patton, F. D. 1966. Multiple modes of shear failure in rock. Proc. 1st Cong. of Int. Soc. Rock Mech. Lisbon. Vol. 1, 509-513.

Potvin, Y. 1988. Empirical open stope design in Canada, Ph.D. thesis. Univ. of British Colombia, Canada, 350p.

Shen, B. & Barton, N. 1997. The disturbed zone around tunnels in jointed rock masses. Technical Note, Int. J. Rock Mech. Min. Sci, Vol. 34: 1: 117-125.

Shen, B., O. Stephansson, and M. Rinnie, 2013. *Modelling Rock fracturing Processes – A Fracture Mechanics Approach Using FRACOD.* Springer, 173p.

Ván, P. and B. Vásárhelyi, 2014. Sensitivity analysis of GSI based mechanical parameters of the rock mass. Periodica Polytechnica, Civil Engineering. 58/4 (2014) 379–386.
APPENDIX

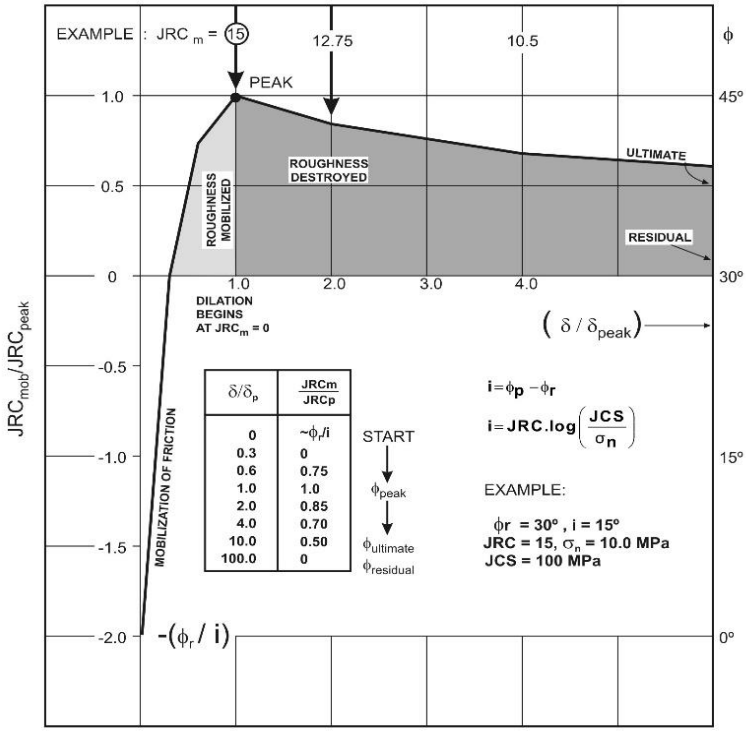

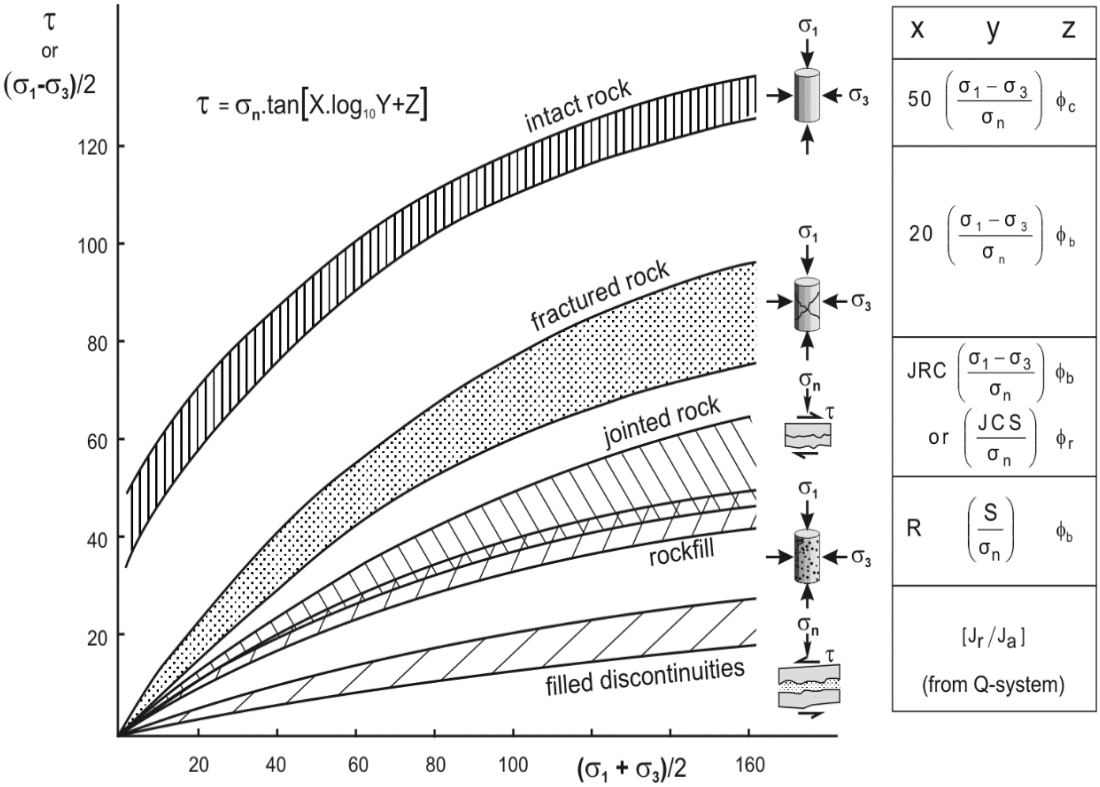

Two of the key items for improved modelling in general. Top: Pre-peak, peak, post-peak mobilization of roughness JRC. Barton, 1982, Barton et al. 1985, Barton, 2013. Bottom: The potential multi-components of progressive failure: CcSs: crack, crunch, scrape, swoosh. Barton 1999, 2006, 2020.